(TITLE - UNCLASSIFIED) CONTROL SURFACE OSCILLATORY COEFFICIENTS MEASURED ON LOW ASPECT-RATIO WINGS

V. BEALS
W. P. TARGOFF

CORNELL AERONAUTICAL LABORATORY, INC.

APRIL 1953

NOTICES

When Government drawings, specifications, or other data are used for any purpose other than in connection with a definitely related Government procurement operation, the United States Government thereby incurs no responsibility nor any obligation whatsoever; and the fact that the Government may have formulated, furnished, or in any way supplied the said drawings, specifications, or other data, is not to be regarded by implication or otherwise as in any manner licensing the holder or any other person or corporation, or conveying any rights or permission to manufacture, use, or sell any patented invention that may in any way be related thereto.

The information furnished herewith is made available for study upon the understanding that the Government's proprietary interests in and relating thereto shall not be impaired. It is desired that the Judge Advocate (WCJ), Wright Air Development Center, Wright-Patterson Air Force Base, Ohio, be promptly notified of any apparent conflict between the Government's proprietary interests and those of others.

WADC TECHNICAL REPORT NO 53-64

SECURITY INFORMATION

(TITLE - UNCLASSIFIED) CONTROL SURFACE OSCILLATORY COEFFICIENTS MEASURED ON LOW ASPECT-RATIO WINGS

V. Beals
W. P. Targoff

Cornell Aeronautical Laboratory, Inc.

April 1953

This bound report is classified "CONFIDENTIAL" and all pages contained therein shall be treated as "CONFIDENTIAL". In the event that any pages become separated or are removed from the main report, each page removed or separated shall be properly marked "CONFIDENTIAL".

Aircraft Laboratory
Contract No. AF33(038)-3384
RDO No. 459-36E

Wright Air Development Center
Air Research and Development Command
United States Air Force
Wright-Patterson Air Force Base, Ohio

McGregor & Werner, Inc., Dayton, O.
100 December, 1953

FOREWORD

The research described in this report was conducted by the Cornell Aeronautical Laboratory, Inc., Buffalo, New York, under Air Force Contract Number AF33(038)-3384.

This project is part of a continuing program of aircraft flutter research sponsored by the Aircraft Laboratory, Wright Air Development Center. The project was administered by Messrs. L. S. Wasserman and W. J. Mykytow of the Dynamics Branch, Aircraft Laboratory, Wright Air Development Center, under Research and Development Order No. R459-36E, Measurement of the Non-Stationary Aerodynamic Pressures Acting on Oscillating Control Surfaces and Tabs of Finite Span (Unclassified).

This document presents experimental research data which has not previously been obtained and which is valuable in conducting more accurate flutter analyses and in establishing flutter design criteria. It is classified RESTRICTED in accordance with par 25b (6), AFR 205-1.

ABSTRACT

Wind tunnel tests were conducted on low aspect ratio wings in order to:

1. Measure the oscillatory aerodynamic lift forces, pitching moments, and hinge moments acting on rectangular wings of aspect ratio 1 and 2, due to the harmonic vibration of flap or tab.

2. Measure similar data due to static deflection of flap or tab.

3. Measure wing pitching moment and flap hinge moment of the finite wings under zero lift conditions.

4. Compare these measured data with existing low aspect ratio theory.

The models were of NACA 0010 section having 5 ft. chords and spans of 2.5 ft. and 5 ft. corresponding (with the reflection plane) to the aspect ratios of 1 and 2 respectively. The wings incorporated full span flap and tab with chords of 40% and 10% wing chord respectively.

Results of the tests are presented in the form of curve sheets with the theoretical comparisons plotted with the corresponding experimental curves.

Most trends indicated by the finite span theory of Refs. 12 and 16 are substantiated by experiment. Quantitative agreement with the theories for wing lift due to both static and oscillatory flap deflection is excellent. However, all measured moments are substantially smaller than those predicted by the theories.

The tests were performed in the Variable Density Tunnel of the Cornell Aeronautical Laboratory, Inc., Buffalo, New York during January 1952.

PUBLICATION REVIEW

This report has been reviewed and is approved.

FOR THE COMMANDER:

for W. O. Lippman
DANIEL D. McKEE
Colonel, USAF
Chief, Aircraft Laboratory
Directorate of Laboratories

TABLE OF CONTENTS

LIST OF FIGURES

SYMBOLS

β	Flap angular deflection relative to wing chord
δ	Tab angular deflection relative to flap chord
ω	Circular frequency of oscillation
V	Air speed
b	Semi-chord of wing, including flap and tab chord
$\frac{V}{b\omega} = \frac{1}{k}$	Reduced velocity
AR	Aspect ratio
L_β	Aerodynamic wing lift coefficient due to oscillations of the flap about its leading edge. (As defined in Ref. 21)
M_β	Aerodynamic moment coefficient about the wing quarter-chord point due to oscillations of the flap about its leading edge. (As defined in Ref. 21)
T_β	Aerodynamic moment coefficient about the flap leading edge due to oscillations of the flap about its leading edge. (As defined in Ref. 21)
T_δ	Aerodynamic moment coefficient about the flap leading edge due to oscillations of the tab about its leading edge. (As defined in Ref. 21)
Q_β	Aerodynamic moment coefficient about the tab leading edge due to oscillations of the flap about its leading edge. (As defined in Ref. 22)
Q_δ	Aerodynamic moment coefficient about the tab leading edge due to oscillations of the tab about its leading edge. (As defined in Ref. 22)
ϕ_{L_β}	Phase angle by which L_β leads β
ϕ_{M_β}	Phase angle by which M_β leads β
ϕ_{T_β}	Phase angle by which T_β leads β
ϕ_{T_δ}	Phase angle by which T_δ leads δ

$\emptyset_{Q_\beta}$	Phase angle by which Q_β leads β
$\emptyset_{Q_\delta}$	Phase angle by which Q_δ leads δ
C_{L_β}	Wing lift coefficient due to static flap deflection
C_{M_β}	Wing moment coefficient due to static flap deflection
$C_{H_{\beta_\beta}}$	Flap hinge moment coefficient due to static flap deflection
$C_{H_{\beta_\delta}}$	Flap hinge moment coefficient due to static tab deflection
$C_{H_{\delta_\beta}}$	Tab hinge moment coefficient due to static flap deflection
$C_{H_{\delta_\delta}}$	Tab hinge moment coefficient due to static tab deflection

INTRODUCTION

Of all cases of flutter actually experienced on full-scale airplanes, those involving a control surface degree of freedom by far are the most numerous. It follows that the determination of the unsteady air forces associated with control surface oscillations are of fundamental interest to the aeroelastician. It is not surprising, therefore, that a substantial literature exists containing various theoretical developments for these forces. However, experiments aimed at verification of the theoretically predicted air forces have been limited.

As reported in Ref. 1, the Cornell Aeronautical Laboratory, under the sponsorship of the USAF conducted tests on a two-dimensional wing-flap-tab combination for the cases of flap or tab oscillating. As a logical extension of that work, the program reported on herein was undertaken to provide additional data for low aspect ratio cases.

The development of methods for calculating the aerodynamic forces acting on an oscillating wing of finite span in an inviscid incompressible flow has occupied numerous investigators, Refs. 2 to 11. These works vary in approach, mathematical rigor, complexity, and results. In general, their basic assumptions are valid only for high aspect ratio wings. Ref. 11 also suggests a method that would be satisfactory for very low aspect ratio wings. The only theory that is claimed by its proponents to be applicable to low aspect ratio wings (say AR's of between one and three) is that of Lawrence and Gerber, Ref 12, and the comparisons made in the body of this report are with respect to this theory.

The foregoing comments relating to oscillatory conditions apply almost equally strongly to the static forces. At the time of initiation of this project, it appeared obvious that experimental static data could probably be obtained from the apparatus designed for the dynamic case with little additional effort, and that such data would be very valuable additions to the relatively small amount of experimental low aspect ratio information available. The theoretical work used for comparative purposes herein are those of Stone, Ref. 16, and DeYoung, Ref. 17, the former report being an application of the theory of Lawrence, Ref. 18.

Having introduced static testing into the program, an additional item of interest appeared worthy of investigation. Lifting line theories trace all finite span effects to the reduction of strength of the bound vorticity. Thus the theory would indicate that for a wing of zero lift, i.e. zero circulation, the wing pitching and flap hinge moments would be unaffected by aspect ratio. Tests permitting the evaluation of this conclusion were made in the program and are discussed in the body of the report.

The objectives of this program may thus be noted formally as:

1. Measurement of the oscillatory aerodynamic lift forces, pitching moments, and hinge moments acting on rectangular wings of aspect ratio 1 and 2, due to the harmonic vibration of flap or tab.

2. Measurement of similar data due to static deflection of flap or tab.

3. Measurement of wing pitching moment and flap hinge moment of the finite wings under zero lift conditions.

4. Comparison of these measured data with existing low aspect ratio theory.

I. DESCRIPTION OF MODELS AND SUSPENSIONS

A. Model

The Variable Density Wind Tunnel of the Cornell Aeronautical Laboratory has a test section 8½ ft. high X 12 ft. wide. All models used in this program were supported as cantilevers from a reflection plane in the top of the test section. Clearance of 1/16 in. was provided between the model root and wind tunnel ceiling. All models were of 5 ft. chord and of NACA 0010 section and were equipped with full span flap and tab hinged at the 60% and 90% chord positions respectively. Models with spans of 2.5 and 5 ft. were used to obtain effective aspect ratios of 1 and 2 respectively. The tab was constructed in such a manner that the outer 50% span could be separated from the inner half and locked to the flap while the inboard section could be deflected. Figures 1 and 2 show the model as installed in the tunnel. Complete description of design details will be found in Appendix I.

B. Suspension

While for many of the tests the wing balance system was locked out, wing lift and pitching moment were measured in certain phases of the program. The operation of the wing balance system is explained in Appendix III. This system was used only to separate and measure wing lift and wing pitching moment; drag force, rolling moment, and yawing moment being discarded. Flap and tab hinge moments were measured by means of strain gage instrumented locking bars. These bars also permitted static variation of flap or tab angle of attack through the range from -8° to $+8^{\circ}$ in two degree increments. For the dynamic tests, either the flap or the tab locking bars were removed and the corresponding surface attached through a universal joint to a motor-driven oscillator that was mounted above the wind tunnel test section ceiling, Fig. 3. Frequency control from 0.5 cps to 6.0 cps was provided by a variable speed drive and half amplitudes of either 4° or 6° were available. The hinge moment of the surface being driven was measured by the torsional deflection of a sensitive section between the oscillator and the universal joint. The hinge moment of the locked surface was measured by means of the strain gages on the locking bars. As discussed in Appendix II, suitable devices were employed to insure that all inertial effects were balanced either mechanically or electrically and that only the aerodynamic hinge moments were recorded.

The wind tunnel test section ceiling to which the model's suspension system attached, was actually a motor-driven turntable. Wing angle of attack control was obtained by simply rotating this turntable. Complete description of the suspension system, oscillator, and associated equipment will be found in Appendix III.

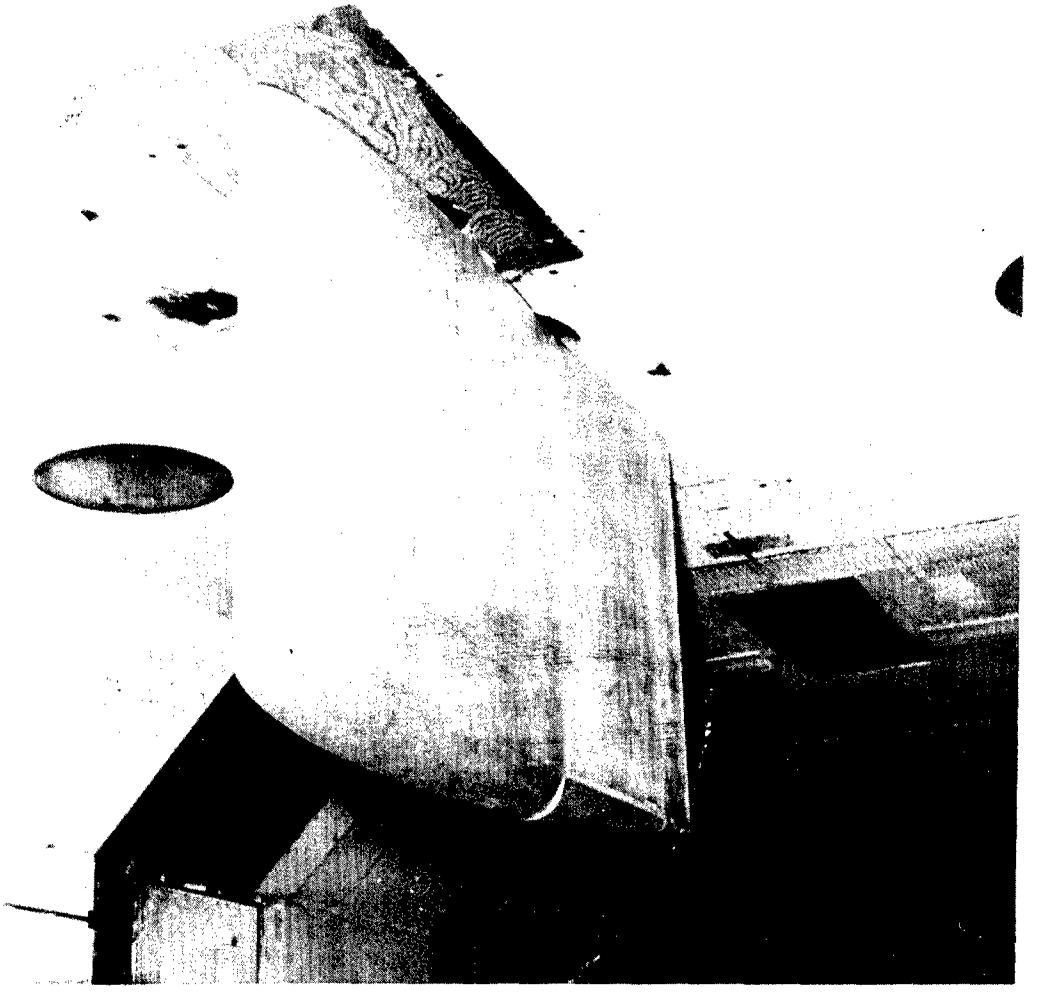

FIG. 1 TUNNEL INSTALLATION
ASPECT RATIO 1 MODEL

FIG. 2 TUNNEL INSTALLATION
ASPECT RATIO 2 MODEL

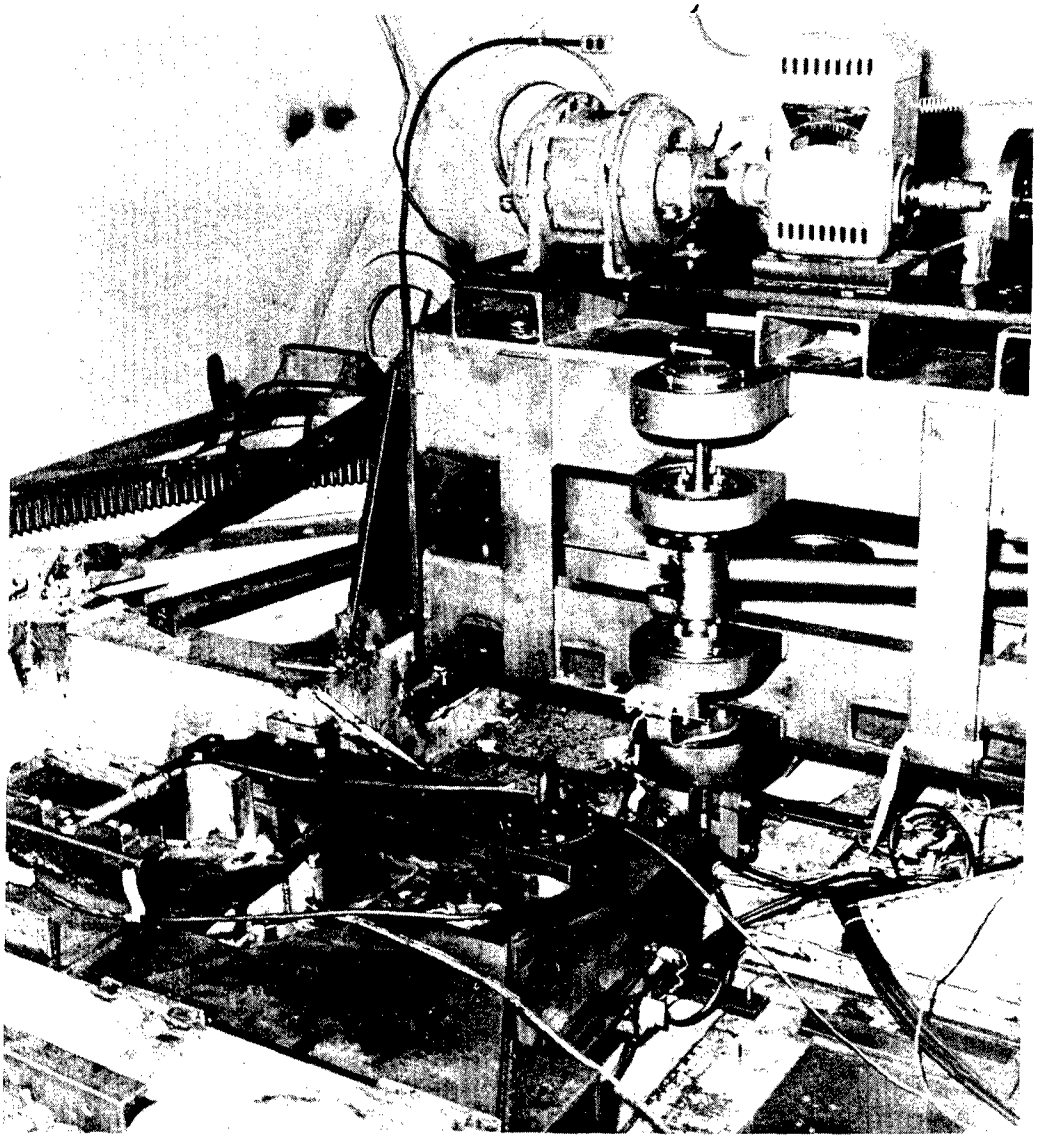

FIG. 3 OSCILLATOR AND WING SUSPENSION SYSTEM

II. CALIBRATION TESTS

A. Static

The measuring devices were calibrated at least twice before their use in the actual wind tunnel test and, in some cases, more than twice. A complete calibration of all the sensitive sections were made with the model set up in the shakedown testing jig, Fig. 4. Just before any particular measuring device was to be used during the wind tunnel test, it was recalibrated. The calibrations made in the shakedown jig were done in both directions (i.e. in the case of a lift load - up and down; and in the case of a moment - clockwise and counterclockwise). With the model mounted in the wind tunnel test section, calibrations were made in only one direction. Since complete calibrations were already available, those run in the wind tunnel served primarily as a check. In all cases, no significant difference between the shakedown and final calibrations was noted.

For all shakedown and wind tunnel calibrations, the wing was mounted vertically as a cantilever. Only concentrated loads were applied to the model.

Wing lift and pitching moment were calibrated by applying a load at the aft wing spar. This provided a moment arm about the elastic axis of approximately 1 ft. A lift range of 0 to 400 lbs. was applied in 25 lb. increments and a pitching moment range of 0 to 400 ft. lbs. in 25 ft.-lb. increments was obtained.

In the case of the wing lift calibration, the load was applied at either of two span-wise stations. It was most generally applied at the center-span of the wing, but, in a few cases, as a check on the effect of rolling moment, it was applied at the root. As was to be expected from the design of the wing balance system, no appreciable change in the lift measurement was observed. Therefore, it was concluded that all rolling moment was being disposed of without affecting other measurements.

The flap locking bars were calibrated by applying a force just forward of the tab hinge line. For the aspect ratio two configurations, two locking bars were used. The calibration was for the effect of the sum of these two bars. For the AR = 1 flap only one locking bar was used. Located at the root, this bar was calibrated separately.

The tab locking bars were calibrated by the application of a load at the trailing edge of the tab. In a similar manner to that noted above, the total effect of the two locking bars was calibrated for the AR = 2 case, and only the root bar was retained for the AR = 1 configuration. This locking bar was calibrated separately.

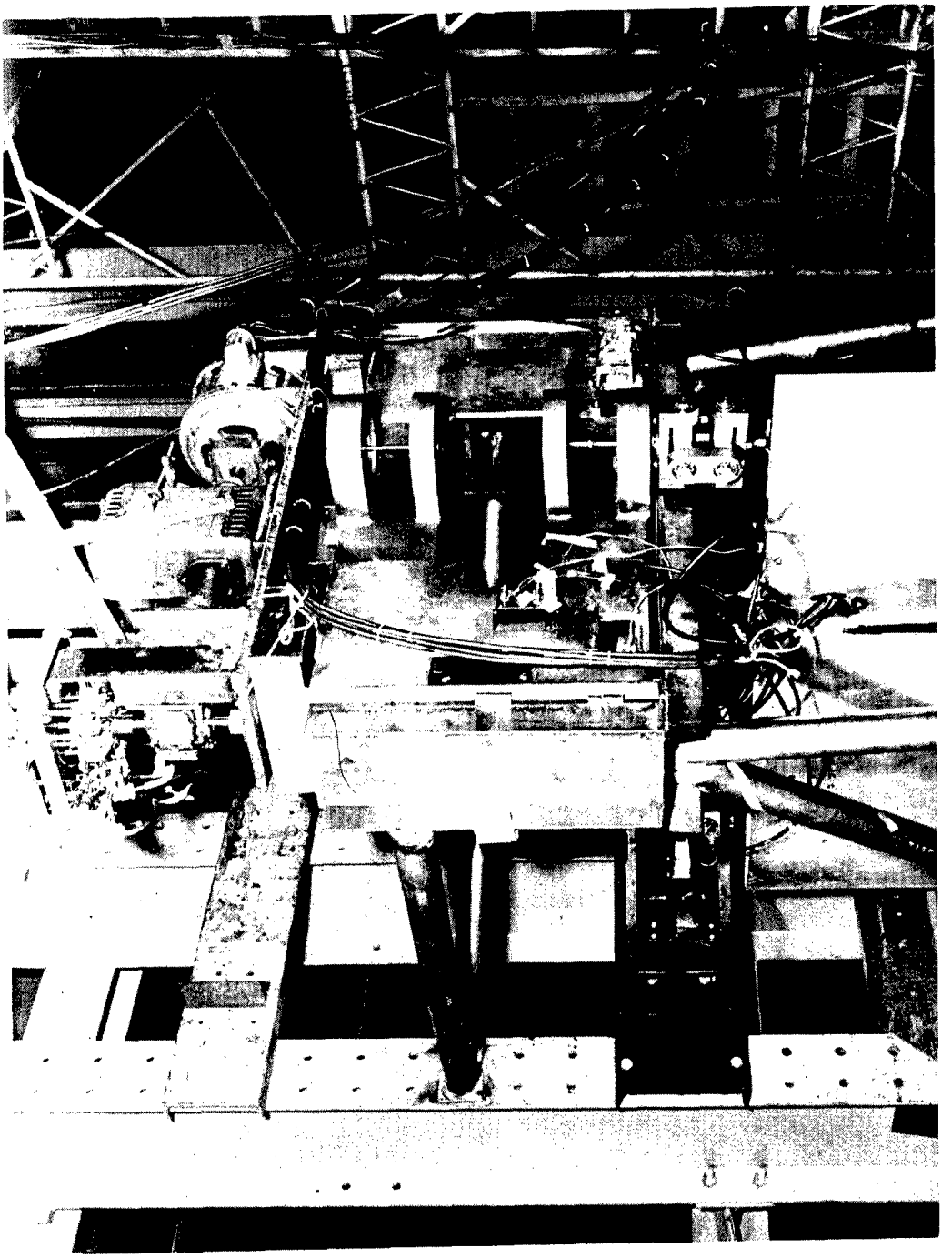

FIG. 4 SHAKEDOWN TEST INSTALLATION

B. Dynamic

For the purpose of calibrating the torque input systems, the wing balance system was locked out. The flap or tab, in turn, was connected to its torque input system and the other control surface locked. Static moments were then applied and thus static calibrations obtained for both tab and flap input sensitive sections. An electrical calibration over the frequency range of interest was performed on the wave filter units used in conjunction with the recording equipment. All other elements of this equipment have no frequency distortion over the range used. The results of the static tests and the electrical filter tests were than combined to give the over-all calibrations.

A Consolidated Engineering Corp. Type 4-104 accelerometer was used as a position indicator for the oscillating control surface. In calibrating this, the surface was driven at the test frequency in still air. By recording the electrical output of the accelerometer and simultaneously permitting a lead pencil, attached to the moving member, to trace a line on a sheet of paper, a direct calibration of the pickup as a position indicator was obtained.

C. Calibration Constants

The following is a tabulation of the calibration factors of the strain sensitive sections. The units are force (or moment) per inch of trace displacement as measured on the oscillograph record. All calibration factors are given for an attemuation of unity.

Wing Lift	15.45 lbs./disp. in.
Wing Pitching Moment	.327 ft. lbs./disp. in.

	Calibration Constant (ft. lbs./disp. in.)	
	AR = 1	AR = 2
Flap Locking Bar	.160	.358
Tab Locking Bar	.0122	.0251
Flap Torque Input	.254	.531
Tab Torque Input	.0150	.0159

These constants are the static values. They were corrected for frequency response by being multiplied by the proper value taken from the calibration curves of the electrical filters. Fig. 5 shows a typical calibration of both magnitude attenuation and phase shift due to the filters.

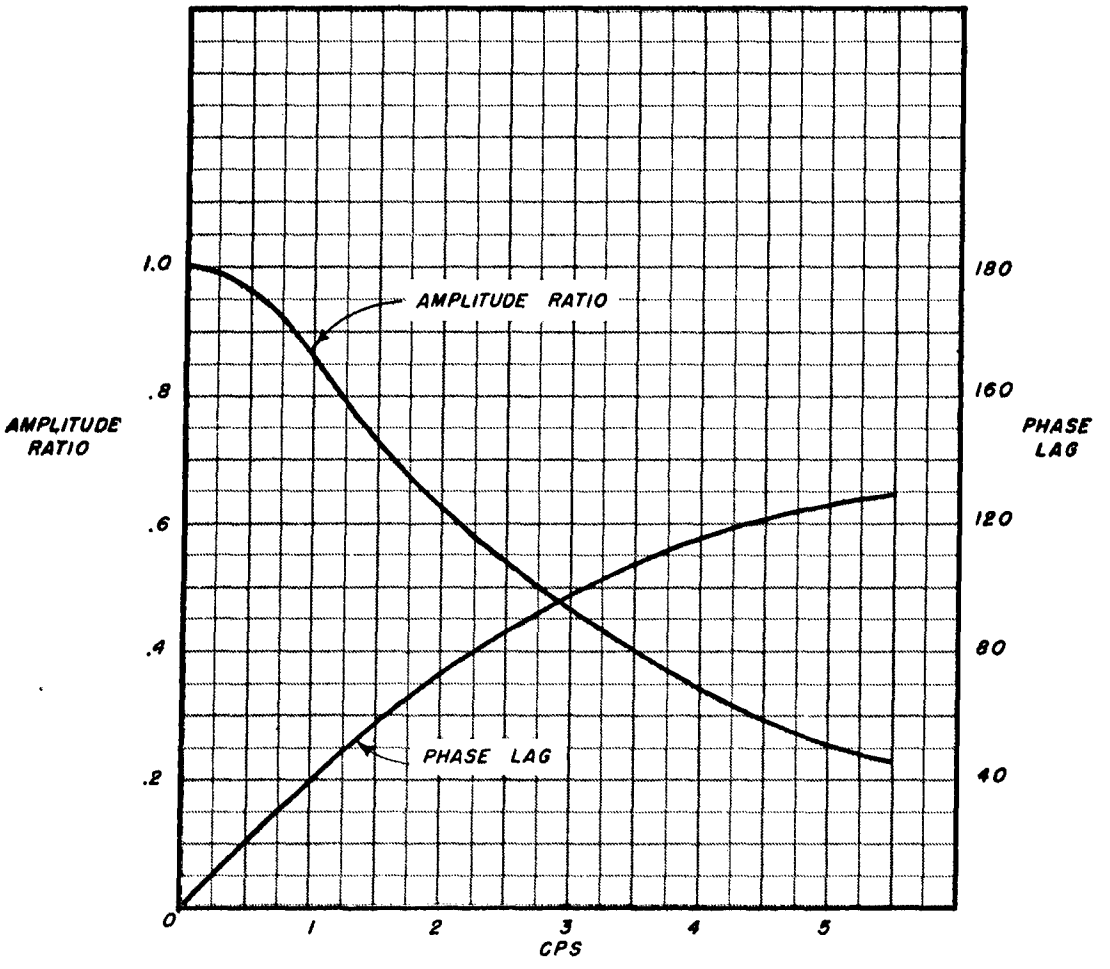

Fig. 5 TYPICAL CALIBRATION CURVE OF FILTER UNIT

III. WIND TUNNEL TESTS

A. General

The wind tunnel program essentially consisted of three phases:

(A) Static tests
(B) Oscillatory tests
(C) Zero lift tests

Three model configurations were tested:

(1) Aspect ratio one model - full span flap and tab
(2) Aspect ratio two model - full span flap and tab
(3) Aspect ratio two model - full span flap, half-span tab

Configuration (3) was subjected only to those tests involving deflection of the tab either statically or dynamically. Configurations (1) and (2) were subjected to the entire test program outlined above.

The wind tunnel tests were all run under ambient atmospheric density conditions which approximate standard sea level density. The Reynolds Number range was from 887,000 to 7,140,000. All wind tunnel tests were conducted in the Cornell Aeronautical Laboratory's $8\frac{1}{2}$ ft. X 12 ft. Variable Density Tunnel during the month of January 1952.

B. Static Aerodynamic Tests

Throughout the entire static program, a standard testing technique was adopted. With the pertinent control surface deflected at a particular angle, data was recorded for the following three conditions:

(1) Tunnel air speed = zero
(2) Tunnel air speed = 125 to 150 mph
(3) Tunnel air speed = zero

Part 1 - Tab Deflections - This part of the static program consisted of deflecting the tab through a range from $+8^{\circ}$ to -8° in 2° increments. This was accomplished by using the tab locking bar as described in Appendix III, (Figs. 6 and 7). All three configurations enumerated above were tested in this manner. The flap was rigidly attached to the wing by means of the flap locking bars. For this particular part of the program, the wing

FIG. 6a TAB LOCKING BAR

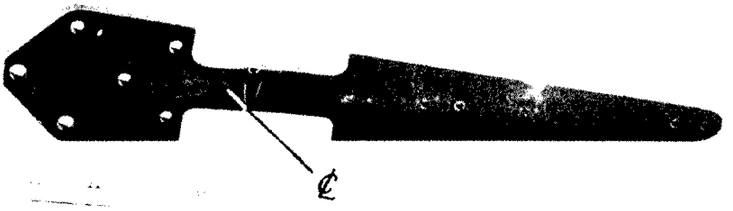

FIG. 6b FLAP LOCKING BAR

UNCLASSIFIED

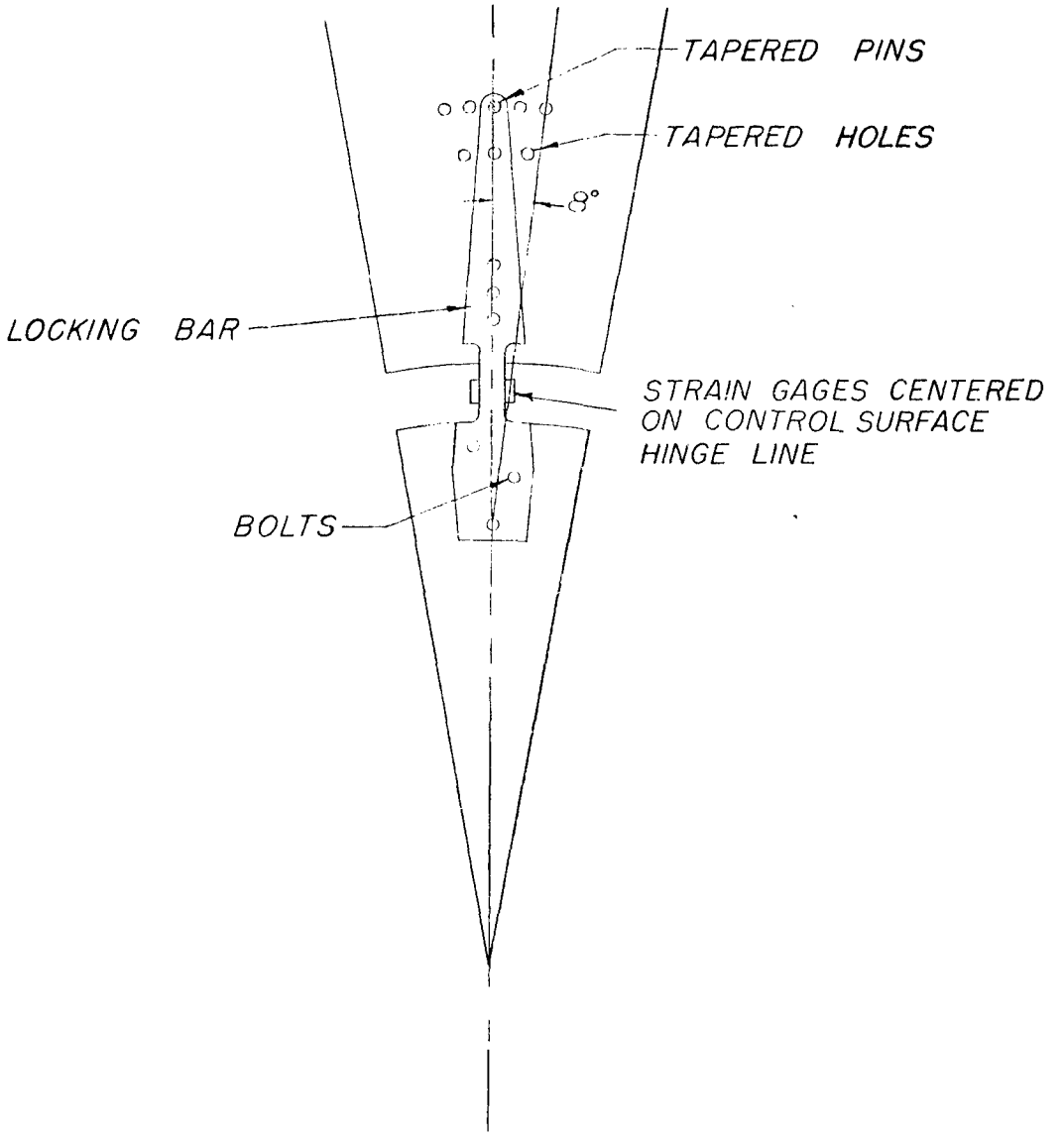

METHOD OF STATICALLY VARYING CONTROL SURFACE ANGLES BY MEANS OF THE LOCKING BARS

FIG. 7

UNCLASSIFIED

balance system was locked out, and only flap and tab hinge moments recorded. The following stationary aerodynamic coefficients were obtained:

$C_{H_{\delta\delta}}$ - Tab hinge moment coefficient due to tab deflection.

$C_{H_{\beta\delta}}$ - Flap hinge moment coefficient due to tab deflections.

Part 2 - Flap Deflections - The flap was set at various angles with respect to the wing by utilization of its locking bars (Appendix III, Figs. 6 and 7). The range of flap angles was $+8^{\circ}$ to -8° in 2° increments. The tab was locked to the flap by the agency of the tab locking bars. The wing balance system was effective and wing lift and pitching moment recorded. Tab and flap hinge moments were measured by the strain-sensitive sections incorporated in the locking bars. Configurations (1) and (2) were tested in this manner. Configuration (2) tests were also made with the balance system locked. These tests yielded the following coefficients:

$C_{H_{\beta\beta}}$ - Flap hinge moment coefficient due to flap deflection.

$C_{H_{\delta\beta}}$ - Tab hinge moment coefficient due to flap deflection.

$C_{M_{\beta}}$ - Wing pitching moment coefficient due to flap deflection.

$C_{L_{\beta}}$ - Wing lift coefficient due to flap deflection.

C. Oscillatory Aerodynamic Tests

A range of reduced velocities from 0 to 3.5 in increments of approximately 0.5 was covered. For the values of reduced velocity between 1.0 and 3.5, an oscillation frequency of approximately 3.0 cycles per second was used and the velocity of the air stream was varied from 30 to 115 mph. Below a reduced velocity of 1.0, it was necessary to increase the oscillation frequency to approximately 5.0 cycles per second.

The testing technique employed in the dynamic phase of the program was as follows. Before commencing the tests, the oscillator frequency control was locked at the desired frequency. The inertia and apparent mass moments acting about the hinge line of the oscillating surface were electronically balanced out with the signal from the accelerometers mounted in the oscillating surface. This electronic balancing

is explained in detail in Appendix II. The readings of the attenuators used to match the accelerometer signal to the signal from the torque input system arising from the mechanical forces were noted. Data was recorded at zero air speed. The tunnel speed was then increased to approximately 30 mph. As soon as the flow was stabilized, data was again recorded. In this fashion, the velocity of the air stream was increased to 115 mph in increments of approximately 15 mph. The tunnel was then shut down and still air data were again recorded as a check on any possible zero shift of the electronic equipment during the testing period.

The oscillatory phase of the program consisted of two parts:

Part 1 - Tab Oscillations - All three model configurations enumerated above were tested in this part of the oscillatory program. Throughout this test, the wing balance system was locked and only flap and tab hinge moments were measured. As explained in Appendix II, the tab was statically balanced for this series of tests which insured that the resultant inertial shear force on the tab due to angular harmonic oscillations about its hinge line was zero, and that the flap hinge moments were of purely aerodynamic origin.

The tab aerodynamic hinge moment was measured by the tab torque input system, the tab initial hinge moment being balanced out electrically.

From this set of tests, the following oscillatory aerodynamic coefficients were deduced:

T_δ - Flap hinge moment coefficient due to tab oscillations.

Q_δ - Tab hinge moment coefficient due to tab oscillations.

Part 2 - Flap Oscillation - Only configurations (1) and (2) were tested in this part of the wind tunnel tests. The tests were made for both the wing locked and unlocked conditions. Only the hinge moment data recorded for the wing locked conditions is presented in the results but the wing lift and pitching moment data were necessarily attained with the wing balance system effective.

The technique described under Part 1 - Tab Oscillation, was also used for the case of flap oscillation. Now, however, the tab was attached to the flap by means of the tab locking bars and the flap hinge moment was measured by the flap torque input system.

For oscillations about the flap hinge line, it was necessary to dynamically mass balance the tab in order to measure the tab aerodynamic hinge moment, and to statically mass balance the flap to measure wing aerodynamic loads (Appendix III).

From these tests, the following oscillatory aerodynamic coefficients were obtained:

T_β - Flap hinge moment due to flap oscillations

Q_β - Tab hinge moment due to flap oscillations

L_β - Wing lift due to flap oscillations

M_β - Wing pitching moment about wing quarter-chord due to flap oscillations

D. Zero Lift Tests

Only model configurations (1) and (2) were tested in this phase of the program and these only for the case of flap deflected.

With the flap and tab at zero deflection, the wing was rotated by means of the turntable in the ceiling of the wind tunnel, until a zero lift condition was obtained. That is, until the lift sensitive galvanometer showed no movement when the air speed was changed from zero to 150 mph. Then with the flap deflected through a specific angle, data was recorded at:

(1) Tunnel air speed = zero
(2) Tunnel air speed = 150 mph
(3) Tunnel air speed = 150 mph. Wing rotated to bring lift channel galvanometer deflection back to that of Condition (1).
(4) Tunnel air speed = 150 mph. Wing rotated back to Condition (2).
(5) Tunnel air speed = zero

Wing pitching moments and flap hinge moments were obtained in these tests for flap angles from -8° to $+8^\circ$ in 2° increments.

IV. DISCUSSION

A. General

The experimental aerodynamic coefficients, measured on the low aspect ratio wings of this program are presented graphically in Figs. 8 through 20. The oscillatory coefficients are presented in terms of:

(a) The magnitude of the aerodynamic coefficient
(b) The phase angle between the aerodynamic vector and the displacement of the surface giving rise to the aerodynamic force,

both versus the reduced velocity ($V/b\omega$). The static aerodynamic coefficients are plotted versus the angular displacement of the deflected surface. All control surface moment coefficients are given about the control surface hinge line; wing pitching moment coefficients are given about the quarter-chord.

All oscillatory aerodynamic coefficients are defined in accordance with Refs. 21 and 22. Static moment coefficients are based on the chord of the surface on which the moment is acting. All coefficients are based on the length of the surface which is deflected.

In all but one instance, the system was sufficiently rigid so that the effect of deformations of the structure and locking bars could be neglected. However, it was observed that the deflections of the wing balance system was sufficient to affect the flap and tab oscillatory hinge moments. For this reason, only oscillatory hinge moment data obtained with the wing locked is presented.

The models used in this program, of course, only approximate the idealized sections upon which the aerodynamic theories are based. Such things as model boundary layer, tunnel reflection plane boundary layer, thickness ratio, gap seal, and surface contour are examples of items which may be of importance in affecting wing pitching moments and control surface hinge moments. For example, in this program the control surfaces have what is normally considered a closed gap. Actually no seal was employed. Only enough clearance was permitted between the fixed and moving surfaces to prevent rubbing during oscillation. The maximum gap was of the order of 0.05 in. on the flap and was smaller than this on the tab. On the basis of the flap chord of 2.0 ft., this corresponds

to a 0.25% gap, which is considered negligible. However, no definite evaluation of the effect of this has been made. Again, in manufacturing the tab trailing edge, a slight bevel was incorporated in the trailing edge angle. This bevel extended about 3/16 in. forward of the trailing edge and was at approximately a 9° angle with the remainder of the tab surface. On a rational basis, this should be too small a bevel to have any measurable effect. However, as discussed under D, below, a possibility exists that it did affect some of the tab results.

It should be noted that the theoretical correlations, in general, appear more satisfactory for the AR = 2 case than for the AR = 1 case. It would appear that many of the physical differences noted above, between the test model and an idealized theoretical model, would be more important for the lower aspect ratio case. For example, tunnel reflection plane boundary layer represents twice the percentage of the span of the AR = 1 model that it does of the AR = 2 model. For the test conditions, this boundary layer is estimated as being between 2 in. and 3 in. thick at the leading edge of the model. Due to diffusion over the 5 ft. chord, a considerably thicker boundary layer probably exists at the model trailing edge.

The data was not corrected for wind tunnel wall effects. In the static case, based on Ref. 14, the maximum correction is of the order of 6%. From Ref. 15 it appears that in the oscillatory case, for the range of $V/b\omega$'s tested, the corrections will be even smaller. It thus appears that in all cases the corrections are not sufficiently large to warrant application.

B. Phase Angles of the Oscillatory Loads

In order to obtain maximum accuracy in the phase angles, the oscillatory records were reduced by a simple six-point harmonic analysis schedule. On each record, data were analyzed at three different time stations and the results averaged to obtain the final value. It is noteworthy that the phase angles obtained for any particular point were for the most part within three degrees of each other.

In all but one case, the measured phase angles may be considered, for practical purposes, adequately described by the two-dimensional theoretical curves. The results of Ref. 12, where employed, check the measured values even more closely. However, Fig. 12, shows that the tab phase angle due to flap oscillation differs from the two-dimensional theory. For the AR = 2 case the theory deviates from experiment above $V/b\omega$ equal to 2. As can be seen from the figure, the two-dimensional results of Ref. 1 show an almost exactly similar trend. For the AR = 1 case, there appears to be a very marked phase angle effect due to aspect

ratio. However, the general shape of the curve, again is very similar to the experimental results of Ref. 1.

C. Magnitudes of the Oscillatory Loads

The oscillatory aerodynamic coefficients are all compared with two-dimensional theoretical values as given in Refs. 20 and 21. In addition, the wing lift and moment coefficients due to flap oscillation are compared with those computed by the finite span theory of Ref. 12. The shaded areas on the curve sheets show the range of results obtained from the two-dimensional experiments of Ref. 1.

From Fig. 8 the wing lift due to flap is seen to check the theory of Ref. 12 very closely. The decrease in oscillatory lift from AR = 2 to AR = 1 appears almost as great as the decrease from AR = ∞ to AR = 2. The wing moment due to flap, Fig. 9, is substantially less than that predicted by Ref. 12. Thus it is indicated that the theory does not sufficiently account for the forward shift of the center pressure.

The flap hinge moment due to flap, Fig. 10, for AR = 2 is seen to differ from the two-dimensional experimental values only above $V/b\omega \approx 2.5$. The AR = 1 values are substantially reduced. From Fig. 11 it may be seen that the flap hinge moments due to tab oscillation for the three cases tested may be delineated by the two-dimensional experimental curve of Ref. 1. This might be expected, perhaps, because of the relatively high aspect ratio of the tab when based on its own chord.

The oscillatory tab hinge moment due to flap, Fig. 12, similarly to Fig. 10, shows that for AR = 2 the values are the same as the experimental two-dimensional below $V/b\omega \approx 2.5$. Again the AR = 1 values are substantially reduced. As in the case of Fig. 11, Fig. 13 shows that for the three cases tested, the tab hinge moments due to tab are all of approximately the same magnitude. However, the two-dimensional results of Ref. 1 here do not follow the same trend but rather are closer to the theoretical. In light of the sharp difference between theory and Ref. 1 shown in Figs. 11 and 12, some question might be raised regarding the failure of Ref. 1 to agree more closely with the results of the present investigation in Fig. 13.

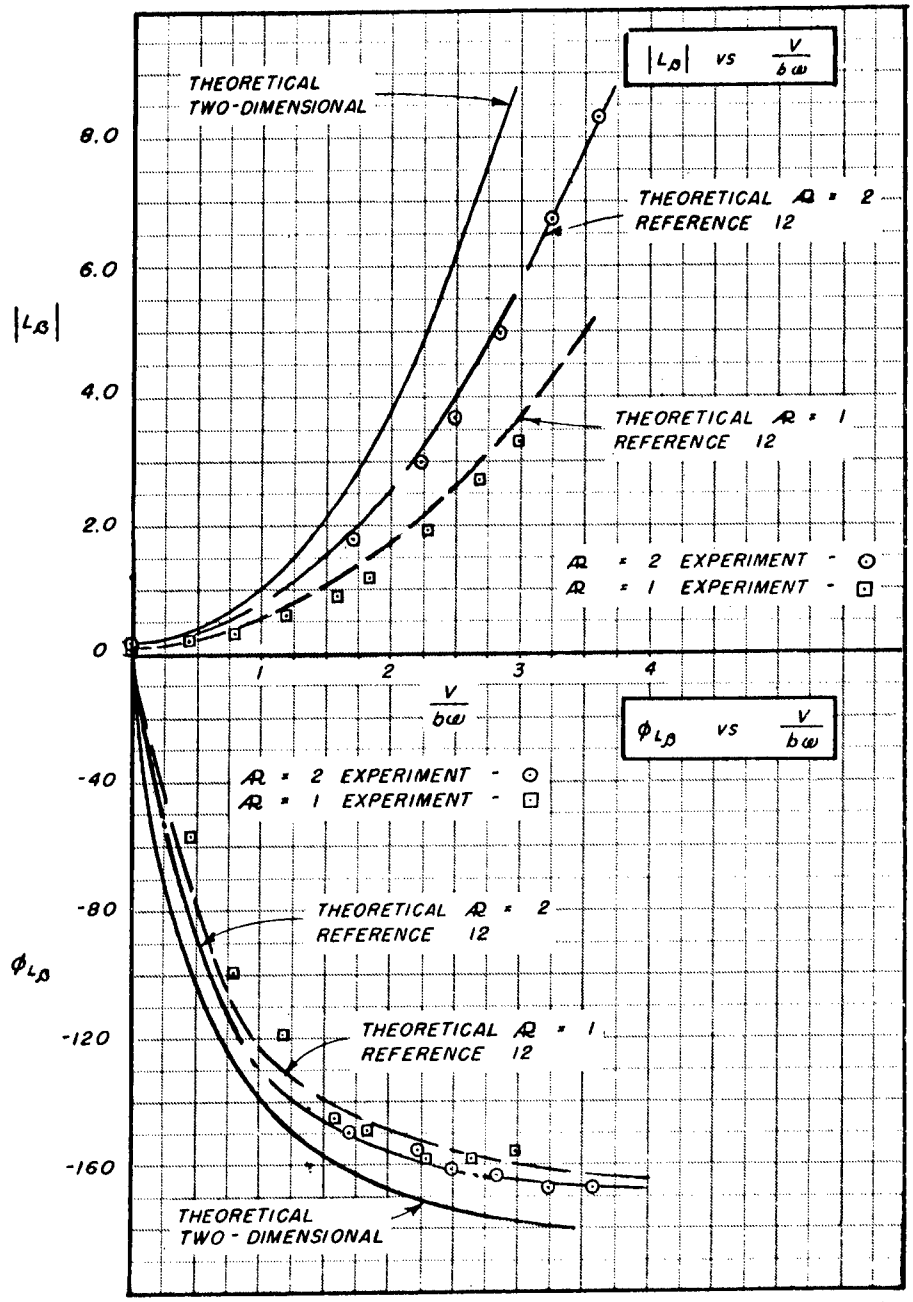

Fig. 8 WING LIFT DUE TO FLAP OSCILLATION

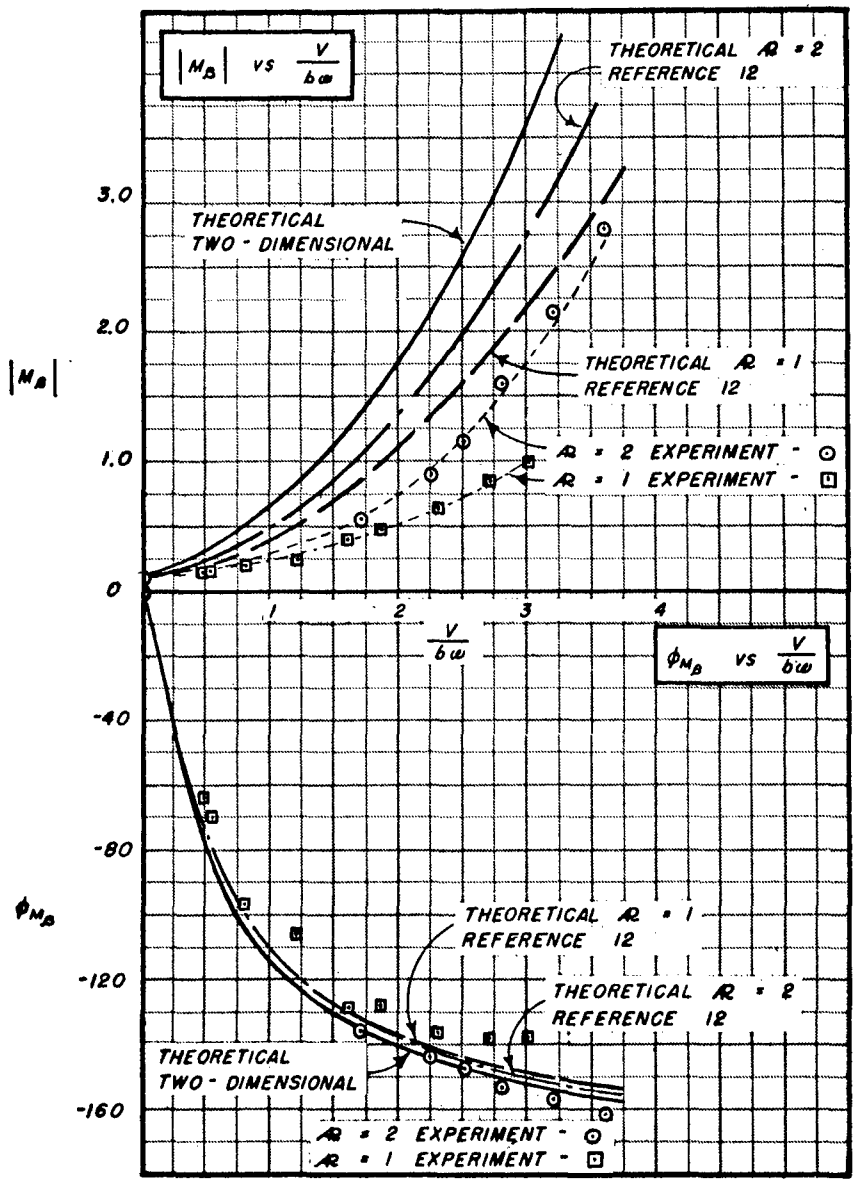

Fig. 9 WING MOMENT DUE TO FLAP OSCILLATION

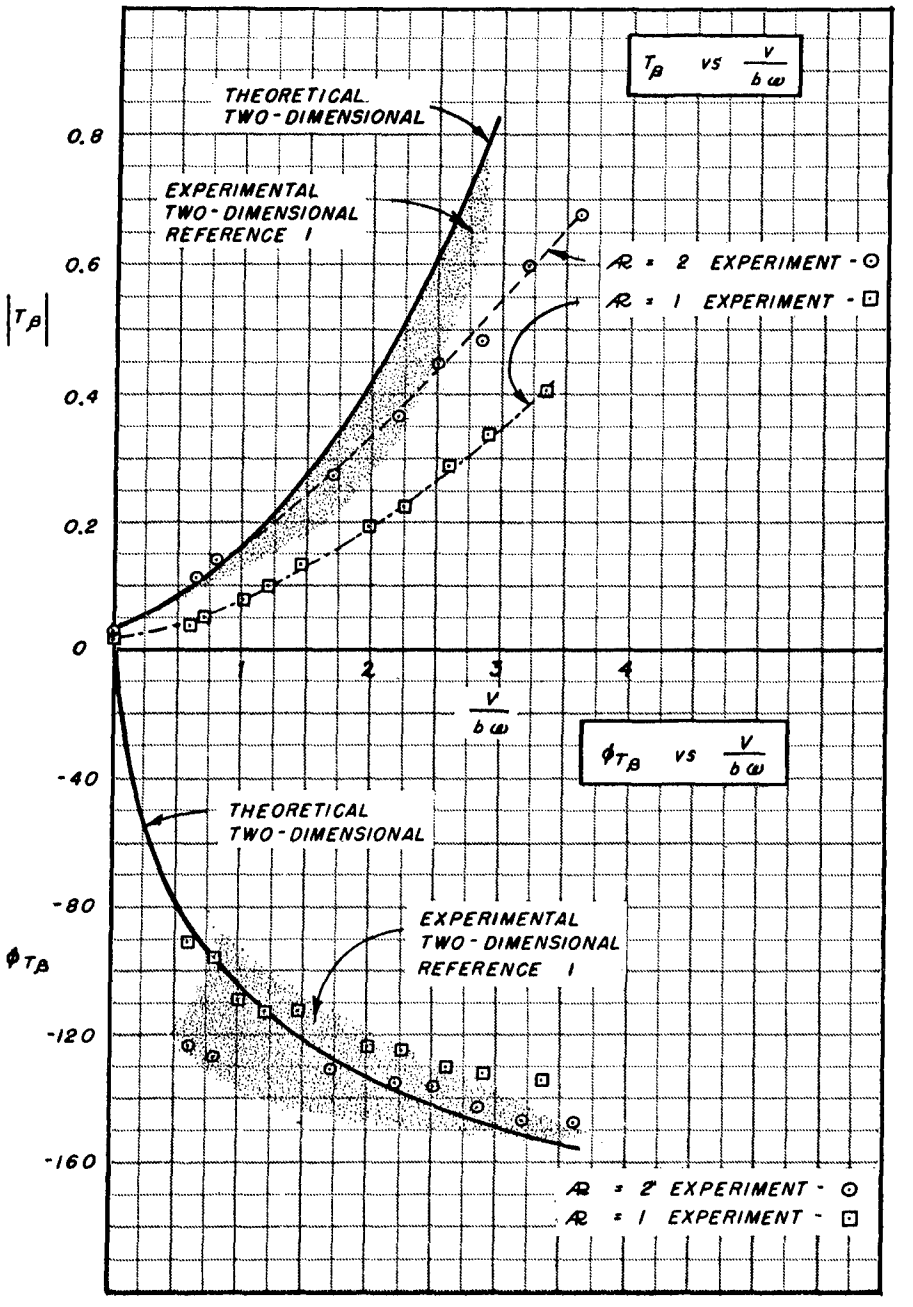

Fig. 10 FLAP HINGE MOMENT DUE TO FLAP OSCILLATION

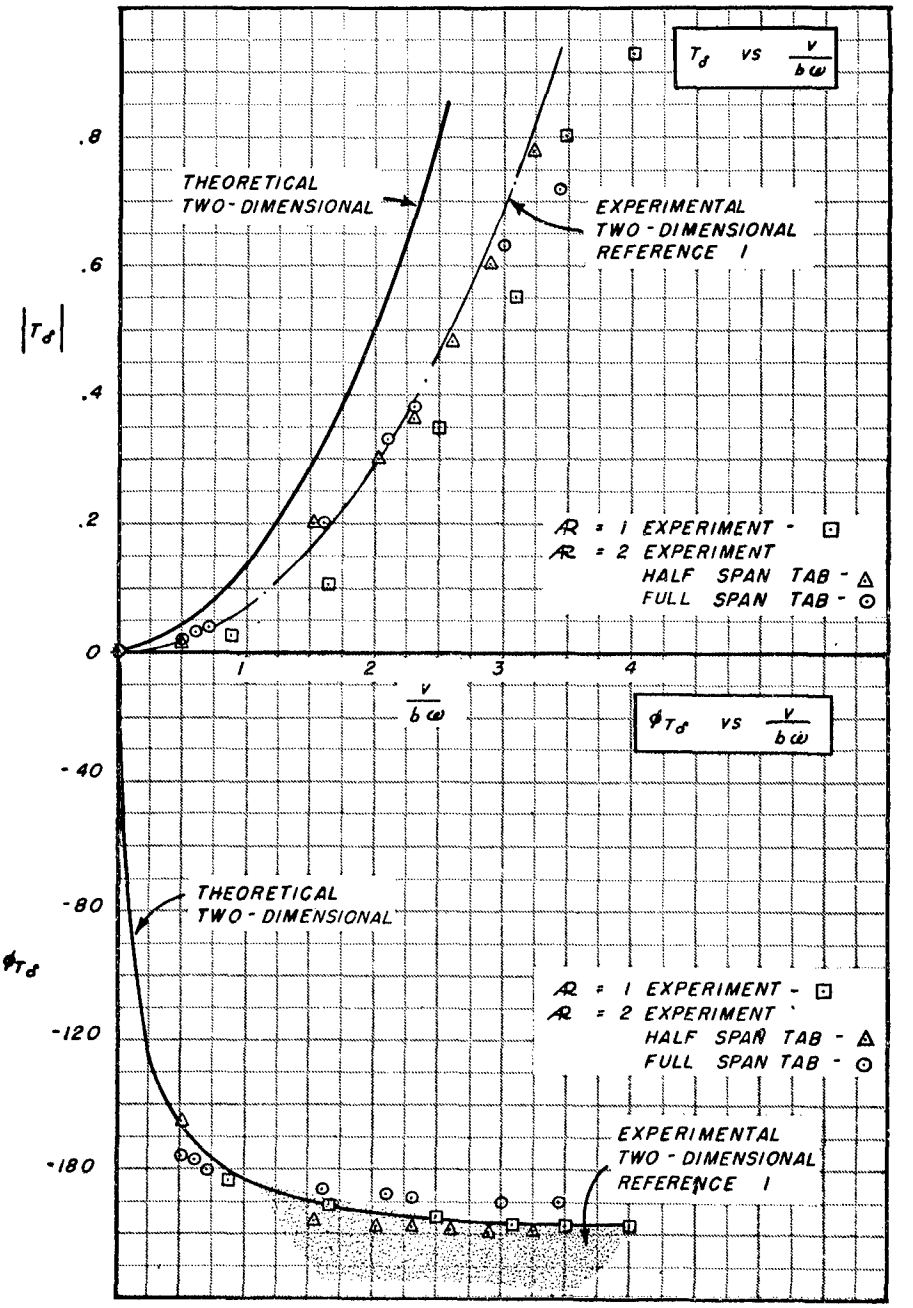

Fig.11 FLAP HINGE MOMENT DUE TO TAB OSCILLATION

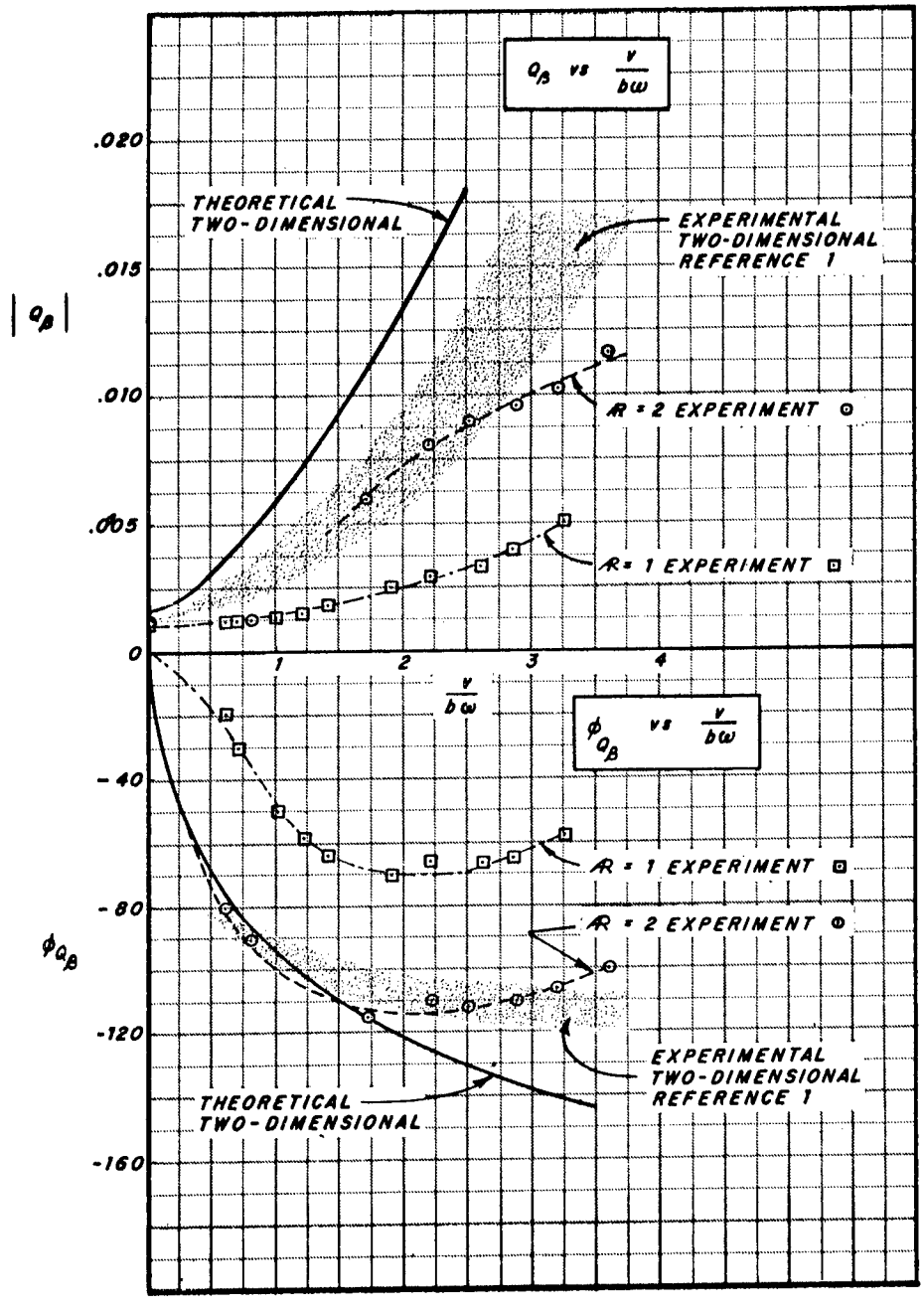

Fig. 12 TAB HINGE MOMENT DUE TO FLAP OSCILLATION

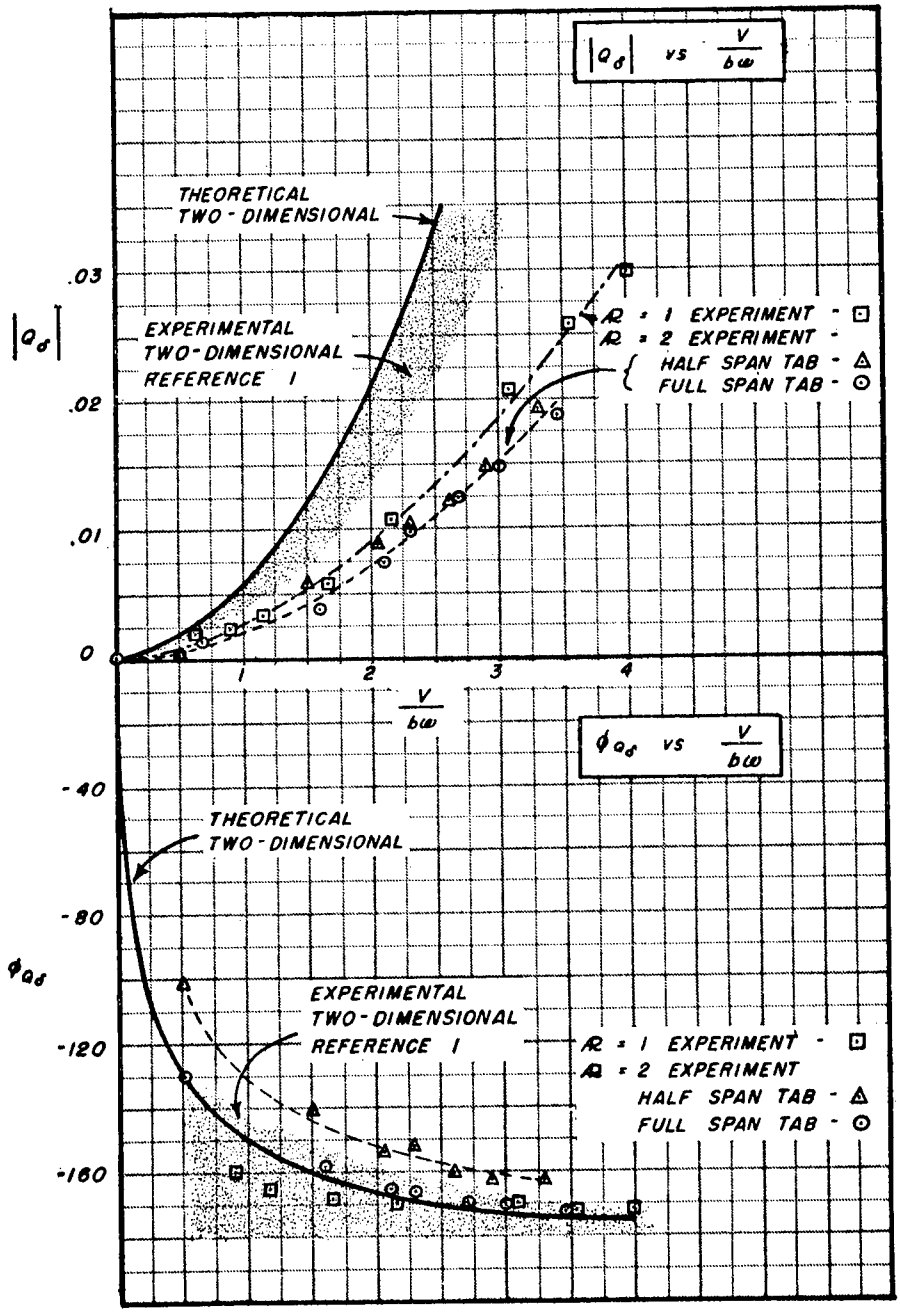

Fig. 13 TAB HINGE MOMENT DUE TO TAB OSCILLATION

D. **Static Loads**

The static aerodynamic coefficients are compared with the finite span theory of Refs. 16 and 18. In addition, the wing lift for the AR = 2 model is compared with the theory of Ref. 17.

The wing lift coefficient due to flap deflection, Fig. 14, checks very closely the theory of Ref. 16 for both the AR = 1 and AR = 2 cases. Ref. 17 for AR = 2, is also shown to be satisfactory. The wing pitching moment due to flap, Fig. 15, is seen to be considerably lower than predicted by the theory, the AR = 1 theory being very close to the actual AR = 2 measurements. For AR = 1 the tests show practically zero wing moment indicating a center of pressure location very close to the quarter chord position.

For the flap hinge moment due to flap, Fig. 16, again the AR = 1 values of Ref. 16 delineate the AR = 2 values of the experiment. The measured AR = 1 moments are approximately one-half the AR = 2 values.

No theoretical comparisons are made for the tab static results as Ref. 16 is based on a six-point collocation and would be highly inaccurate for a model with a 10% tab. Figs. 17 and 18 require almost no comment except for the $C_{H_{\delta_t}}$ curve. This coefficient starts off with the reverse of the expected load direction and then curves back to a normal slope. Two possible explanations of this phenomenon are possible. One is that at this low aspect ratio negative pressures occur on the trailing edge of the flap, probably at the wing tips. The change in slope would then be due to the normal non-linear effects noticed on low aspect ratio wings due to the cross-flow drag. Alternatively the phenomenon may be due to the small bevel on the trailing edge of the tab. While as noted in Ref. 25, this is usually only observed on control surfaces with large bevels, it should be noted that the measured coefficients are of extremely small magnitude, and the effect may have been overlooked in previous experimentation.

Reference should be made to the phase angle of the comparable oscillatory coefficient ϕQ_β. As was pointed out previously, this is the only phase angle that differs appreciably from the theoretical two-dimensional values. It would appear from Fig. 12 that if the curves were extended to high values of $V/b\omega$, they would approach the zero phase lag condition. Remembering that the static value is equivalent

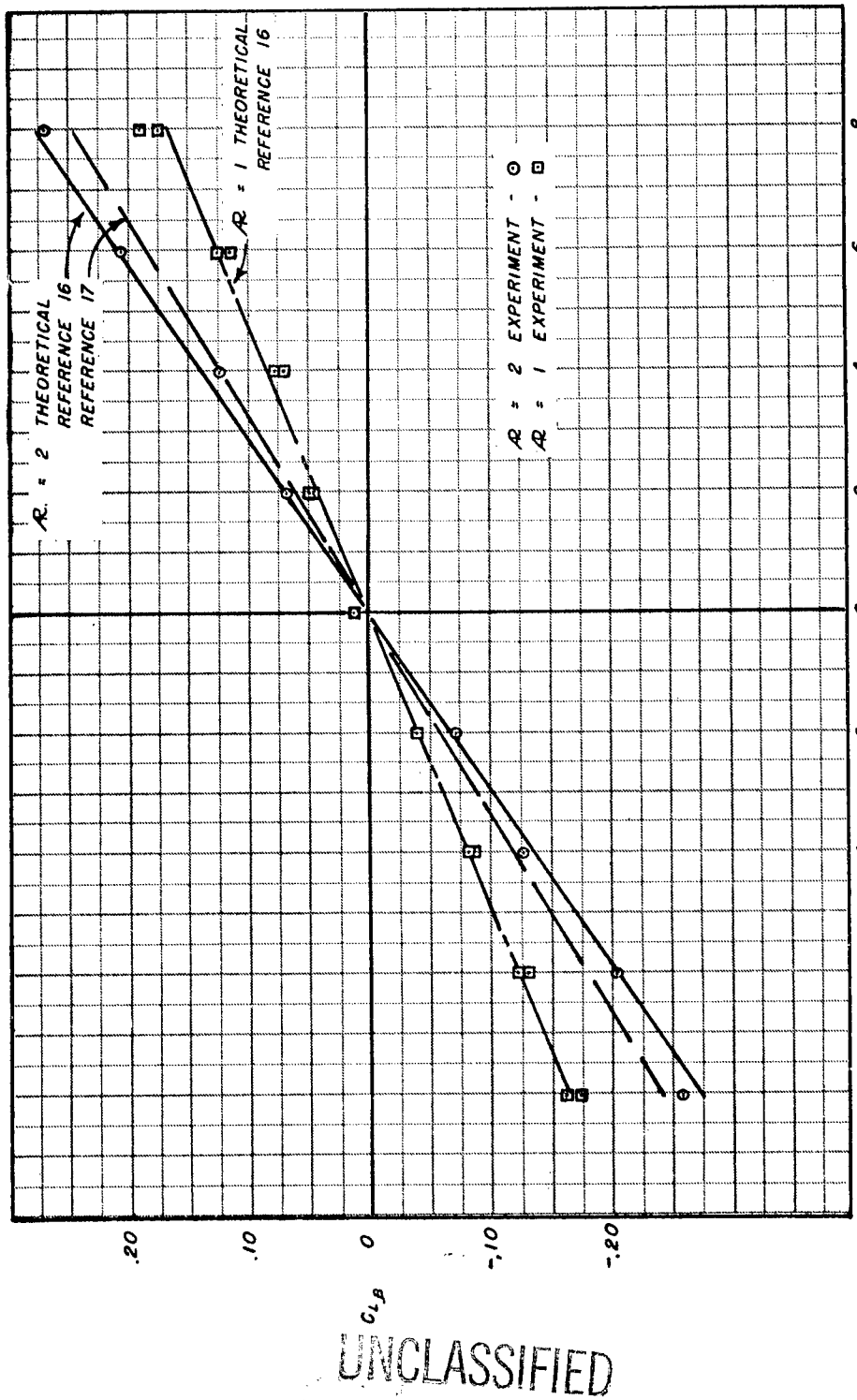

Fig. 14 WING LIFT COEFFICIENT DUE TO FLAP DEFLECTION

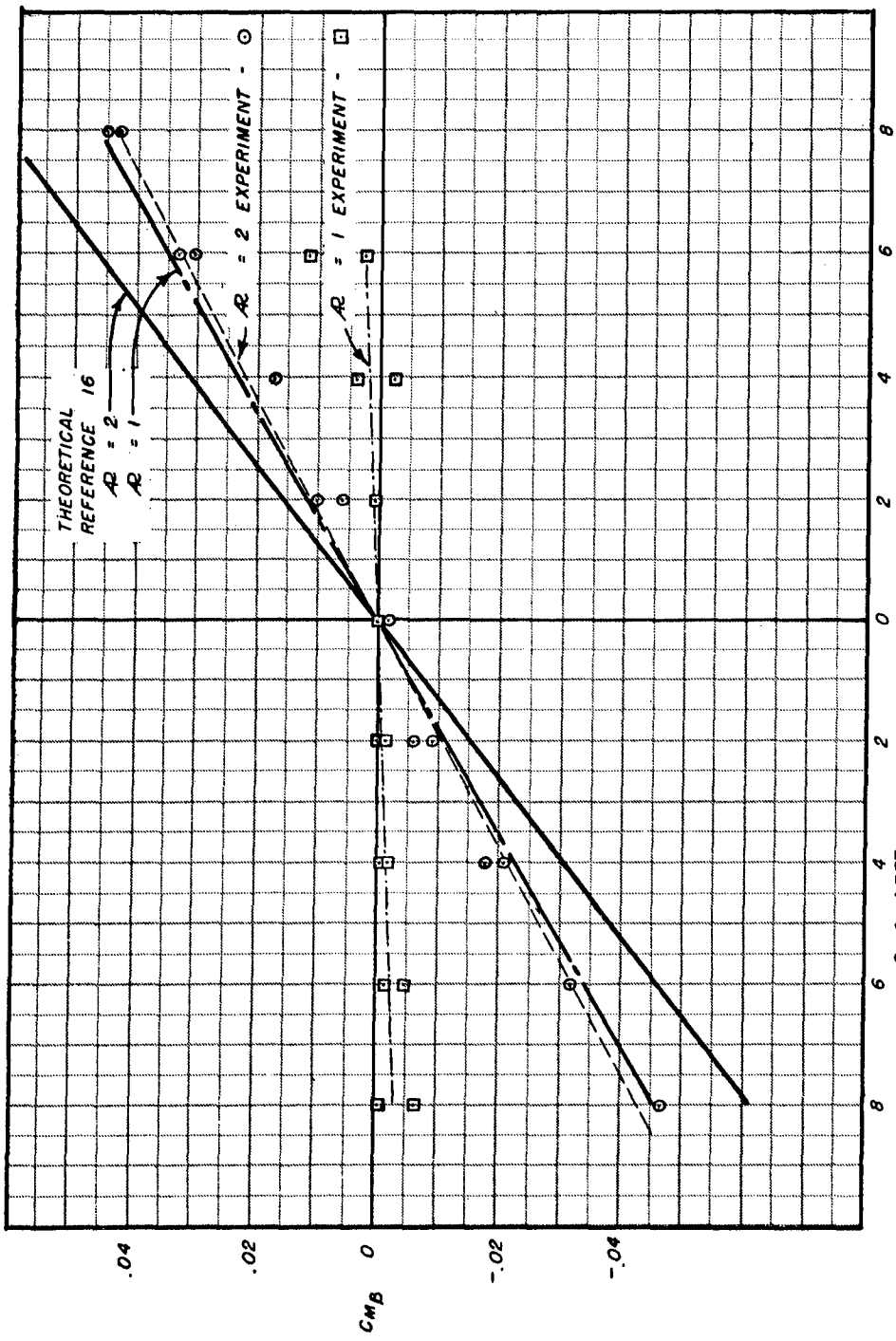

Fig. 15 WING PITCHING MOMENT COEFFICENT DUE TO FLAP DEFLECTION

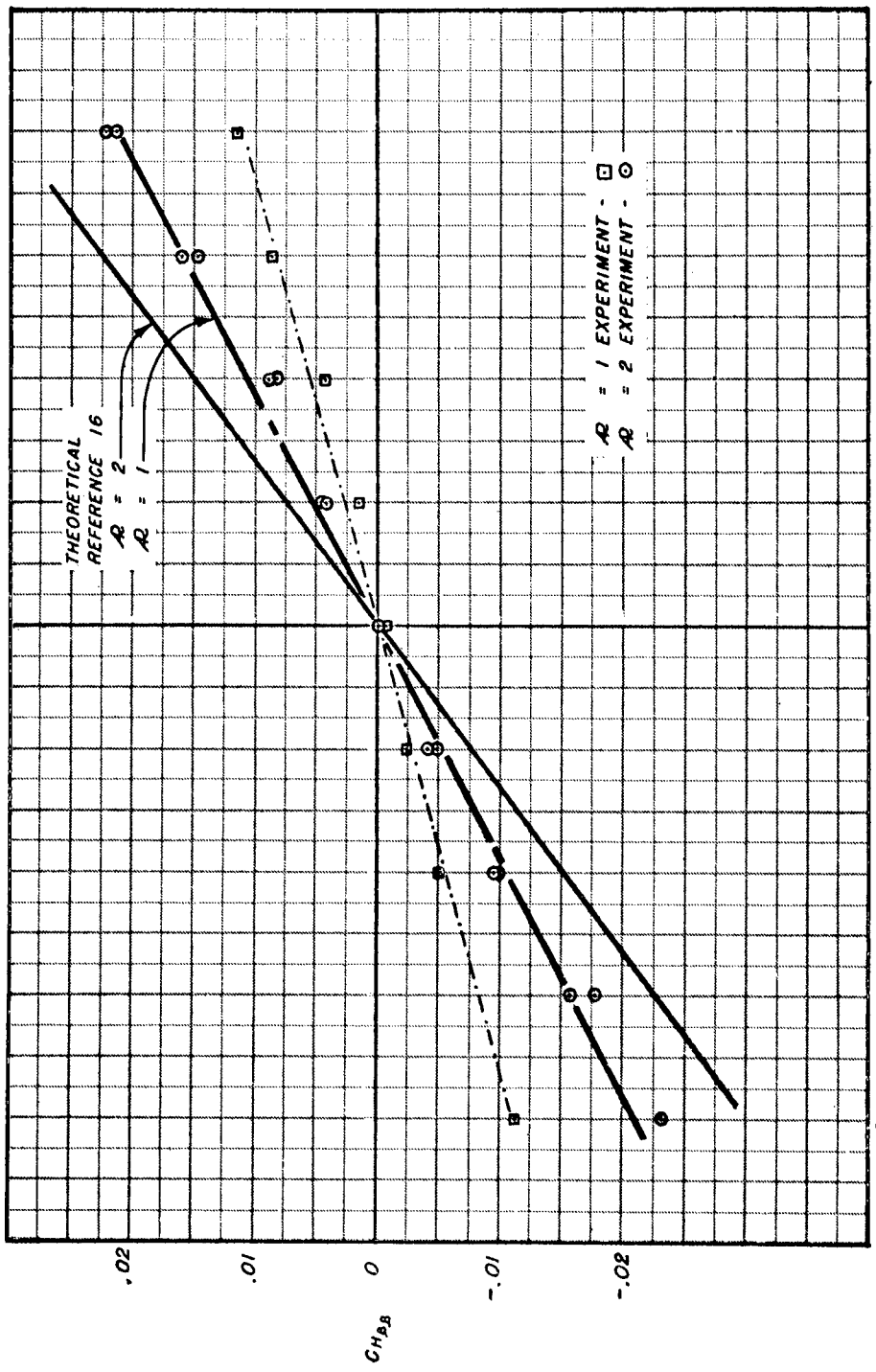

Fig. 16 FLAP HINGE MOMENT COEFFICIENT DUE TO FLAP DEFLECTION

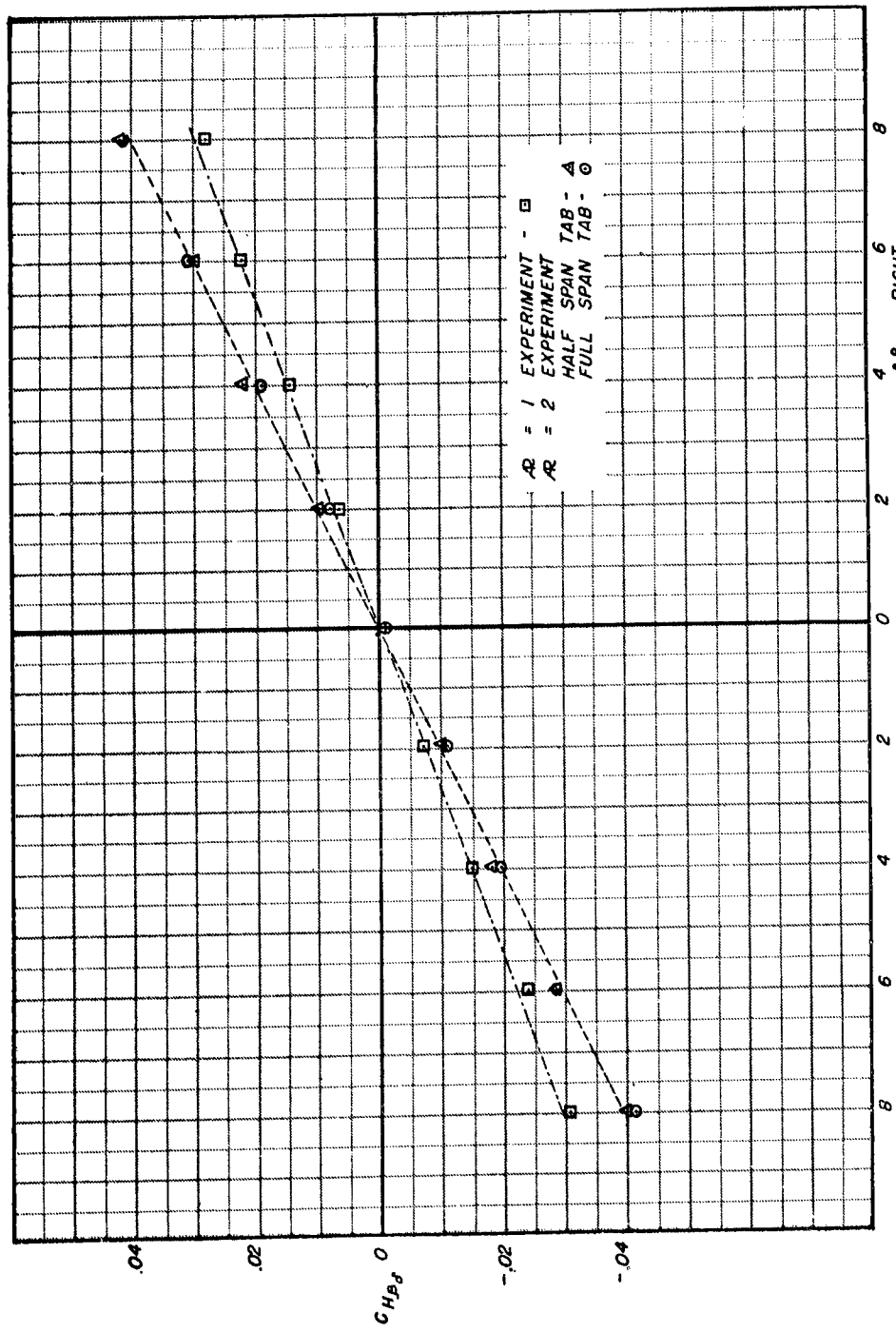

Fig. 17 FLAP HINGE MOMENT COEFFICIENT DUE TO TAB DEFLECTION

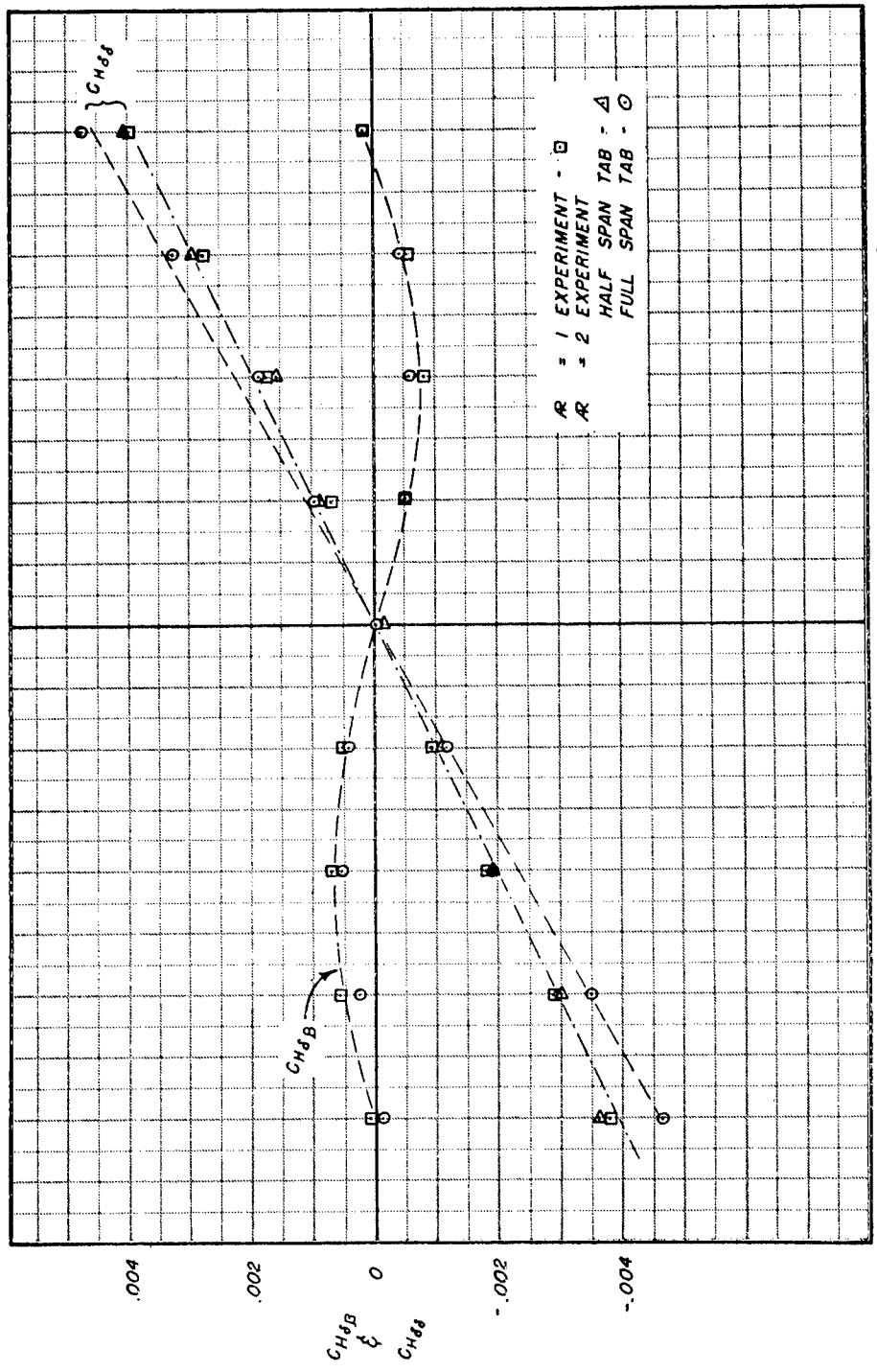

Fig. 18 TAB HINGE MOMENT COEFFICIENT DUE TO FLAP AND TAB DEFLECTIONS

to infinite $V/b\omega$, the approach to zero phase angle means that the static hinge moment would be in the same direction as a static deflection. This, of course, is just what was observed in the static tests.

As in the dynamic cases, there is little difference in the tab coefficients as measured for the three different configurations tested.

E. Zero Lift Tests

Figs. 19 and 20 give wing pitching moment and flap hinge moment for flap deflection, with the wing rotated to a position of zero net lift on the total surface. Comparison of these results with those for the non-rotated wing, Figs. 15 and 16, show little change due to the reduction in lift.

At the zero lift condition, there still exists a marked difference in the moments for the AR = 1 and AR = 2 cases. Thus it would appear that those finite span theories, which are predicated on circulation strength, are inadequate at these low values of aspect ratio.

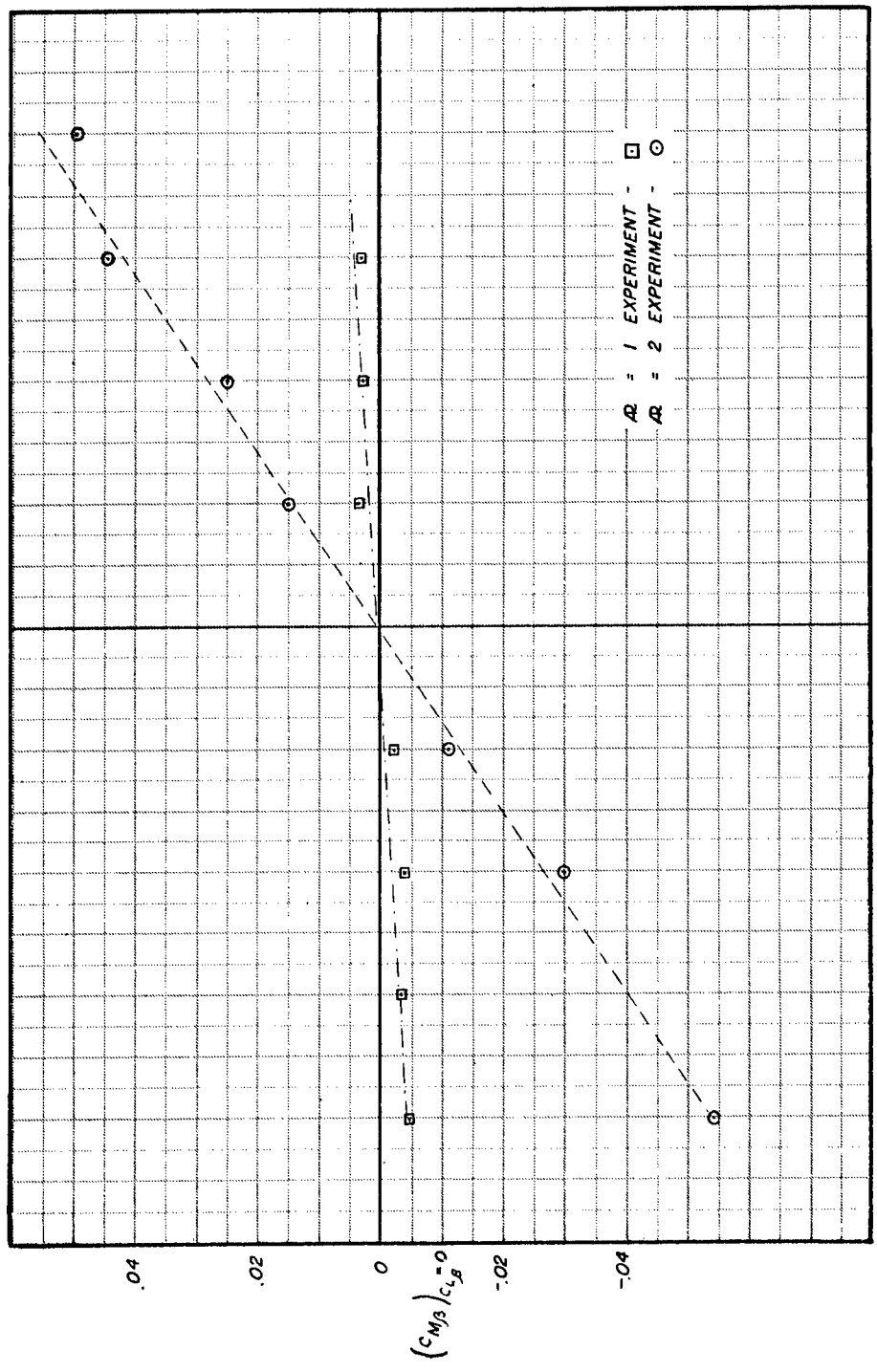

Fig. 19 WING PITCHING MOMENT COEFFICIENT DUE TO FLAP DEFLECTION - AT ZERO LIFT

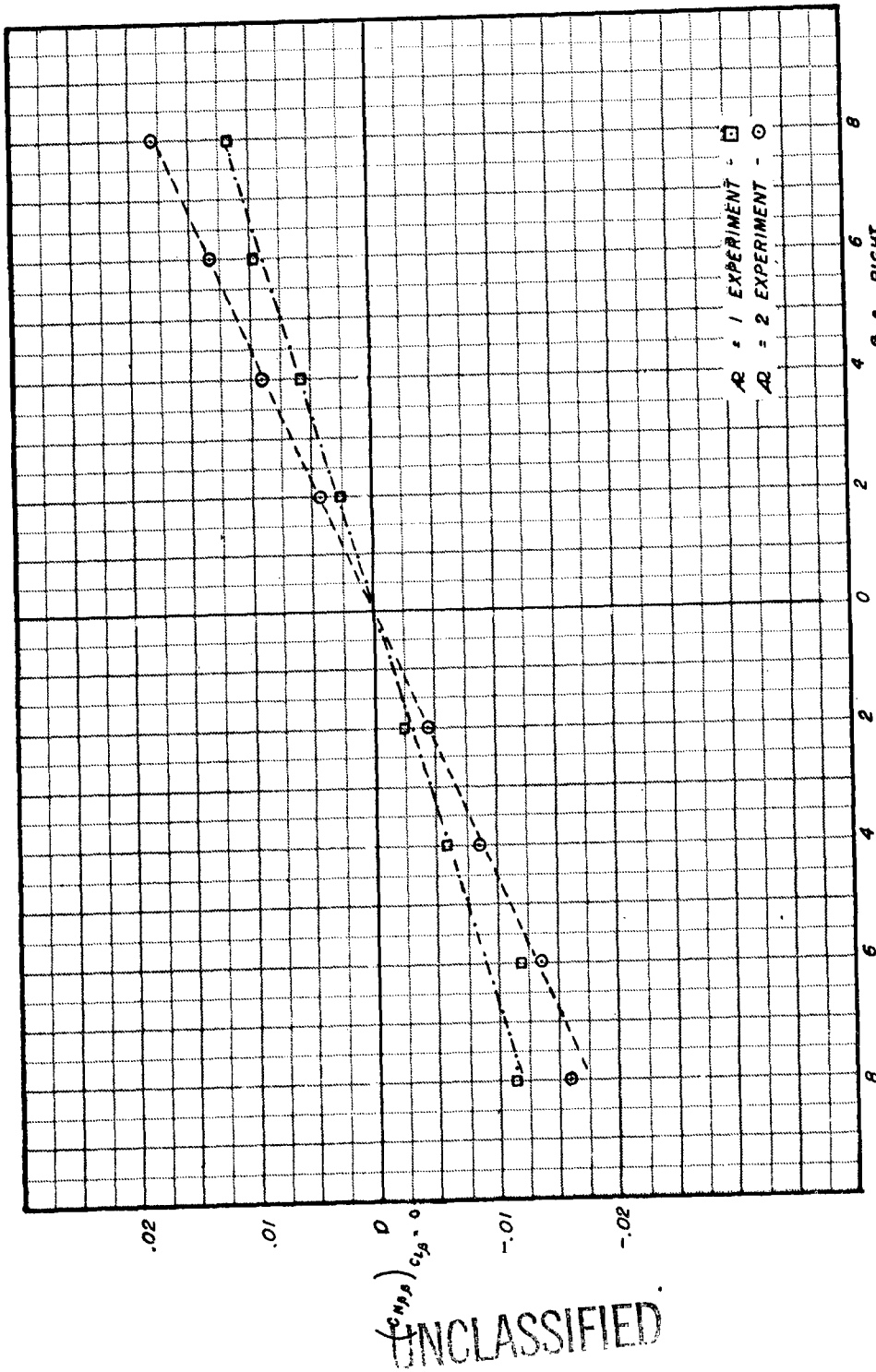

Fig. 20 FLAP HINGE MOMENT COEFFICIENT DUE TO FLAP DEFLECTION — AT ZERO LIFT

V. CONCLUSIONS AND RECOMMENDATIONS

On the basis of the observed data as summarized in the curve sheets, the following general conclusions may be made:

(1) The oscillatory phase angles are only slightly affected by aspect ratio, most of the data falling within the range of two-dimensional values reported in Ref. 1. A notable exception is ϕ_{Q_β} for AR = 1.

(2) The magnitudes of the oscillatory loads are, in general, substantially below the theoretical two-dimensional values. However, T_β and Q_β for AR = 2 and T_δ for AR = 1 and 2 fall within the range of data reported in Ref. 1.

(3) Hinge moments caused by tab oscillation in the three different configurations tested exhibit little difference in magnitude, indicating that the aspect ratio of the control surface itself rather than that of the wing may be of fundamental importance.

(4) The theory of Ref. 12 gives excellent checks of the lift due to flap oscillation both in magnitude and phase angle but overestimates the wing moment due to flap oscillation. However, ϕ_{M_β} is predicted satisfactorily.

(5) The theory of Ref. 16 gives excellent checks of the lift due to static deflection but overestimates all the moments for which comparisons were made. In general, the theoretically predicted moments for AR = 1 compare favorably with the measured data at AR = 2.

(6) As in the oscillatory cases, the hinge moments caused by static tab deflection exhibit only little difference in magnitudes for the three configurations tested.

(7) The results of the static zero lift tests indicate that finite span theories based on total circulation strength are inadequate at low aspect ratios.

In evaluating the results of this series of experiments, consideration should be given to the fact that the indicated wing and tab moments due to flap motion, static and oscillatory, were of very small magnitude. Therefore, the possibility of errors in these results should not be overlooked. However, from the consistency which was exhibited by these values, as measured, it would appear that the magnitudes of the measurement errors were small.

It is recommended that further measurements be made to investigate the effects of:

(1) Gap

(2) Trailing edge angle

(3) Aerodynamic balance

(4) Thickness ratio

(5) Boundary Layer (Both on the model and on the reflection plane)

(6) Compressibility

The effect of compressibility on control surface oscillatory aerodynamic coefficients is considered of fundamental importance. Experimentation in the high subsonic and transonic range is particularly desirable in light of the lack of any suitable aerodynamic theory and the several recent actual cases of control surface flutter at these speeds.

VI. REFERENCES

1. Andreopoulos, T. C., Cheilek, H. A. and Donovan, A. F. Measurements of the Aerodynamic Hinge Moments of an Oscillating Flap and Tab USAF TR 5784 April 1949 (Restricted)

2. Cicala, P. Comparison of Theory with Experiment in the Phenomenon of Wing Flutter L'Aerotecnica Vol. XVIII No. 4 April 1938 NACA TM 887 February 1939

3. Borbely, V. Über einen Grenzfall der instationären räumlichen Tragflügelströmung Z.F.A.M.M. Bd. 18 Heft 6 pp. 319-342 December 1938

4. Dingel, and Küssner, H. G. Contributions to Non-Stationary Wing Theory VIII - The Vibratory Wing of Large Aspect Ratio AMC Translation Report No. F-TS-935-RE

5. Jones, R. T. The Unsteady Lift of a Finite Wing NACA T.N. No. 682 January 1939

6. Reissner, E. Effect of Finite Span on the Airload Distributions for Oscillating Wings I - Aerodynamic Theory of Oscillating Wings of Finite Span NACA T.N. No. 1194 March 1947

7. Reissner, E. and Stevens Effect of Finite Span on Airload Distributions for Oscillating Wings NACA T.N. No. 1195 October, 1947

8. Biot, M. A. and Boehnlein, G. T. Aerodynamic Theory of the Oscillating Wing of Finite Span GALCIT Report No. 5 for the Army Air Forces 1942

9. Chiarulli, P. Oscillating Wings of Finite Aspect Ratio TR-102 AC 49/9-100 AMC USAF 1949

10. Wasserman, L. S. Aspect Ratio Corrections in Flutter Calculations M.R. MCREXA5-4595-8-5 August 1948

11. Garrick, I. E. Some Research on High Speed Flutter, Proceedings of the Third Anglo-American Aeronautical Conference, Appendix B; R. Ae. S-IAS 1951

12. Lawrence, H. R. and Gerber, E. The Aerodynamic Forces on Low-Aspect-Ratio Wings Oscillating in an Incompressible Flow Cornell Aeronautical Laboratory Report No. AF-781-A-1

13. Johnson, H. S. and Hagerman, J. R. Wind Tunnel Investigation at Low Speeds of an Unswept Untapered Semispan Wing of Aspect Ratio 3.13 Equipped with Various 25-Per cent-Chord Plain Flaps NACA TN 2080 April 1950

14. Glauert, H. The Elements of Aerofoil and Airscrew Theory

15. Goodman, Theodore R. The Upwash Correction for An Oscillating Wing in a Wind Tunnel Cornell Aeronautical Laboratory Report No. AD-744-W-1 July 1951

16. Stone, H. N. Aerodynamic Characteristics of Low-Aspect Ratio Wings with Various Flaps at Subsonic Speeds Cornell Aeronautical Laboratory Report No. AF-743-A-2

17. DeYoung, J. Theoretical Symmetric Span Loading Due to Flap Deflection for Wings of Arbitrary Plan Form at Subsonic Speeds NACA TN No. 2278 January 1951

18. Lawrence, H. R. The Lift Distribution of Low-Aspect-Ratio Wings at Subsonic Speeds Journal of Aeronautical Sciences Vol. 18, No. 10 pp. 683-695 October 1951

19. Weissinger, J. The Lift Distribution of Swept-Back Wings NACA TM No. 1120 March 1947

20. Durand, W. Aerodynamic Theory Vol. 1, p. 302

21. Smilg, B. and Wasserman, L. S. Application of Three-Dimensional Flutter Theory to Aircraft Structures AAFTR No. 4798 July 8, 1942

22. Wasserman, L. S., Mykytow, W. S., and Spielberg, I. Tab Flutter Theory and Applications AAFTR No. 5153 September 1, 1944, (Restricted)

23. Reissner, E. Wind Tunnel Corrections for the Two-Dimensional Theory of Oscillating Airfoils Cornell Aeronautical Laboratory Report SB-318-S-3 April 22, 1947

24. The C.A.L. 12-Foot Variable Density Wind Tunnel Airflow Calibration Program, Phase I - Cornell Aeronautical Laboratory Report No. 510238-4 June 2, 1948 p.3

25. Sears, R. I. Wind-Tunnel Data on the Aerodynamic Characteristics of Airplane Control Surfaces NACA ACR 3L08 December 1943

APPENDIX I

DESCRIPTION OF MODELS AND DESIGN DETAILS

The Variable Density Wind Tunnel of the Cornell Aeronautical Laboratory has a test section 8½ ft. high X 12 ft. wide. All models used in this program were supported as cantilevers from a reflection plane in the top of the test section. Clearance of 1/16 in. was provided between the model root and wind tunnel ceiling. The model was equipped with an end fitting which extended through a hole in the wind tunnel ceiling and was attached to the wing suspension system. The wing suspension system and the oscillator were mounted on top of the tunnel ceiling. All models were of 5 ft. chord and of NACA 0010 section and were equipped with full span flap and tab hinged at the 60% and 90% chord positions respectively. Models with spans of 2.5 and 5 ft. were used to obtain effective aspect ratios of 1 and 2 respectively. The tab was constructed in such a manner that the outer 50% span could be separated from the inner half and locked to the flap while the inboard section could be deflected. The control surfaces had effectively a closed gap and zero aerodynamic balance.

The construction details of the aspect ratio 1 and 2 wings were entirely similar, being semi-monocoque, two-spar structures. The spars, slightly modified 5 in. X .225 in. extruded 24ST channels, were located at the 15.94% and 46.98% chordlines and were attached to the skin with counter-sunk machine screws. Ribs built-up of a 1/8 in. 24ST web with two pairs of 1/8 in. X 1 in. X 1 in. 24ST extruded angles riveted to the web to provide cap strip material, were located at the flap hinge stations to transfer the shear load from the flap to the wing skin. These intermediate ribs were interrupted by the continuous spar. A tip rib was provided that was continuous from the wing leading edge to the flap hinge line. Its construction was the same as the intermediate ribs' except that only one angle was used for each capstrip. In the AR = 1 wing, the outboard hinge rib became the tip rib and no special tip rib was required. At the root, a discontinuous rib was provided to transfer the wing loads to the end fitting. Flap hinge fittings were machined from 24ST bar. All the ribs were attached to the spars by means of angles riveted to both the rib and the spar. Two 1/4 in. 61ST6 sheets formed to the contour of an NACA 0010 airfoil section were screwed to the framework described above and welded to each other along the leading edge of the wing. A fairing provided a smooth contour at the tip of the wing. As can be seen from the above description, an extremely rugged design was employed. Figs. 21 and 22 show the basic structure of the two models prior to covering.

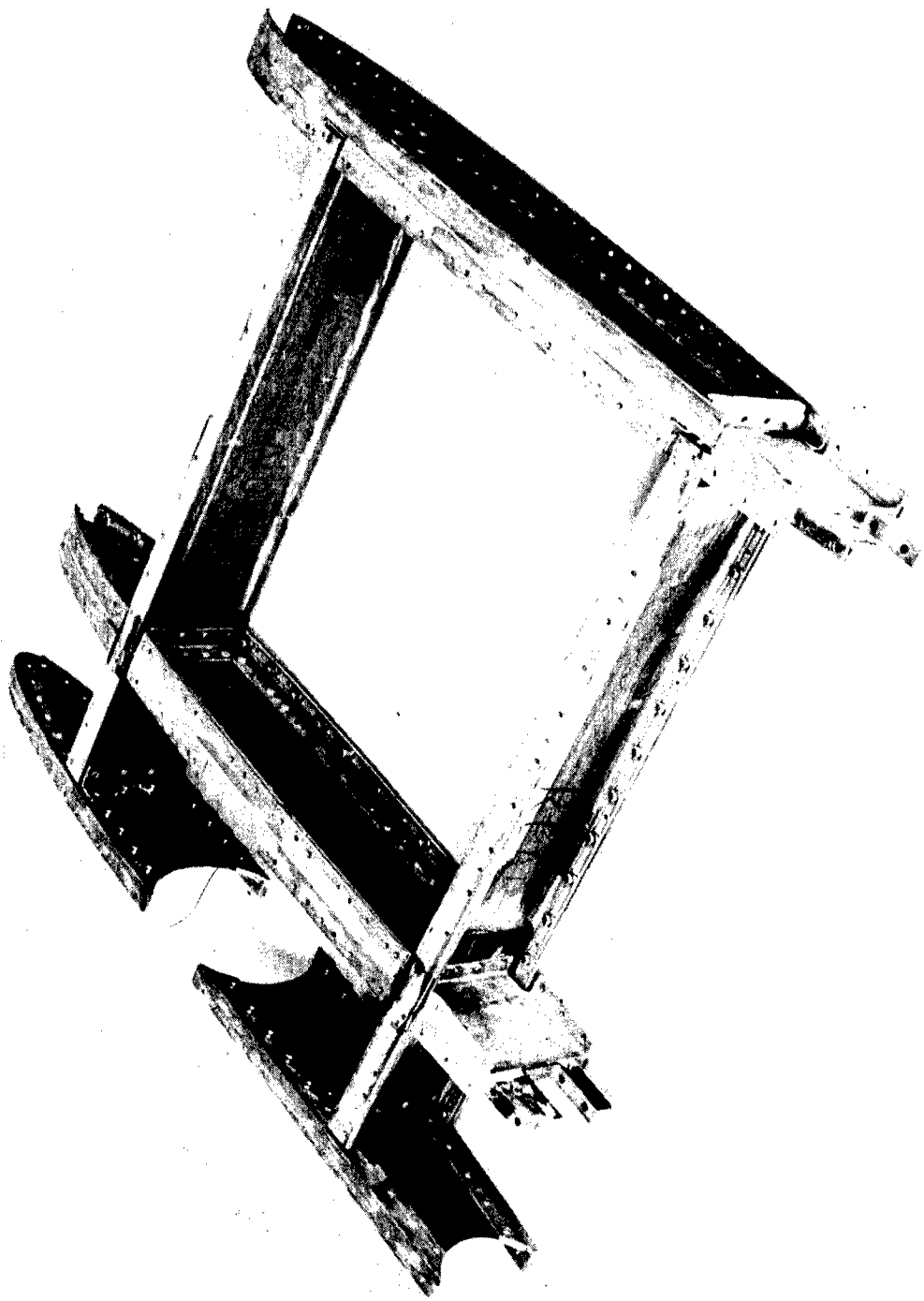

FIG. 21 BASIC STRUCTURE OF ASPECT RATIO 1 WING

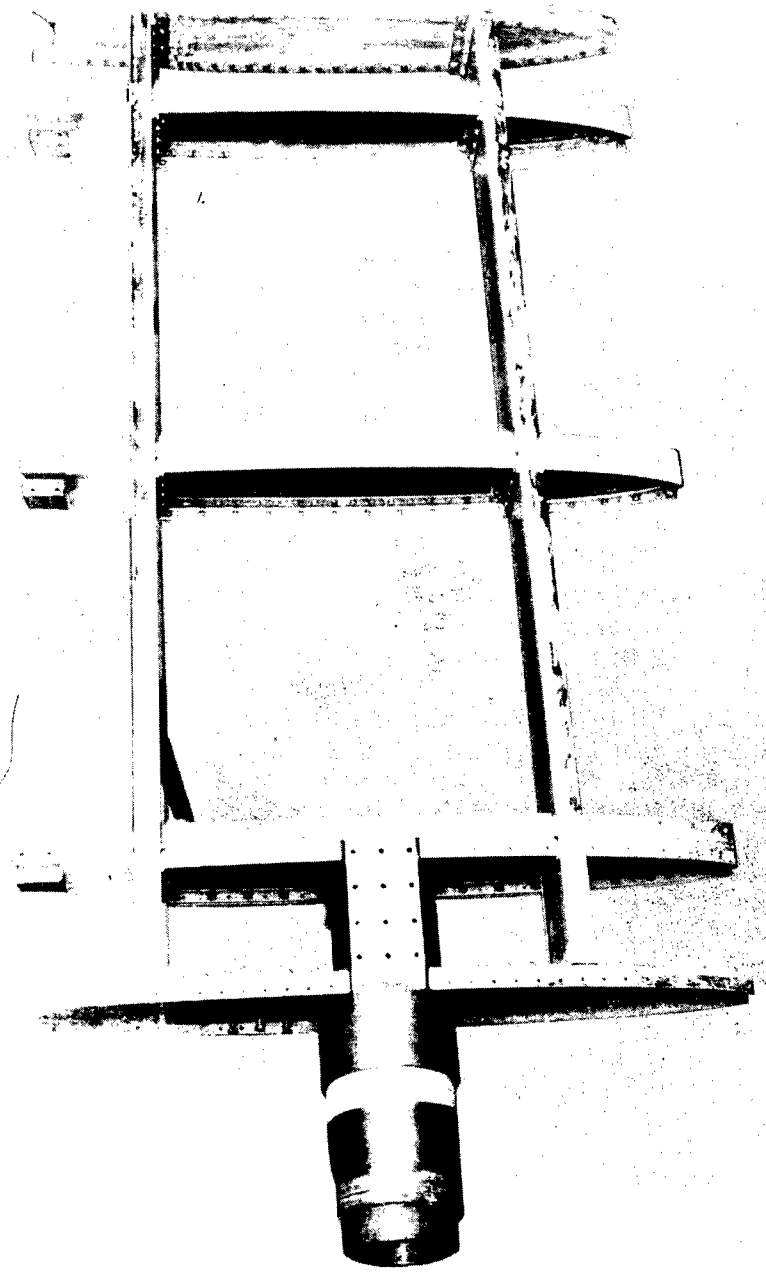

FIG. 22 BASIC STRUCTURE OF ASPECT RATIO 2 WING

The flap was constructed in two parts. When joined, the two pieces formed a full span three-hinge flap for the AR = 2 wing. The two components of the flap were connected by splice plates screwed to both skins. In addition, the outboard nose rib of the inboard section was bolted to the ballast weight of the outboard section. For the AR = 1 wing only, the inboard two-hinge portion was used. A semi-monocoque two-spar type of construction was used. The spars were formed of .040 in. 24ST sheet with flanges bent-up to provide bending material. Ribs intermediate between the spars were formed from .040 in. 24ST. Nose ribs were made of bent-up .064 in. 24ST sheet. The heavier stock in the nose ribs was required to support the large ballast weights used in mass balancing the flap. Two nose ribs were used at the hinge stations to provide support for the hinge bearing shaft. Two trailing edge formers made of 3/8 in. magnesium bar stock, were located between each tab hinge to stiffen up the trailing edge flap panels. Tab hinge supports were machined from 5/8 in. magnesium stock. Ribs, formers, and hinge supports were attached to the flap spars with angles riveted to both the spar and the particular stiffener. Two .051 in. dural sheets formed to the NACA 0010 contour were riveted to the framework.

Figs. 23 and 24 show the flap before covering and in the process of covering. The flap is shown in its split configuration and its joined configuration. Fig. 25 shows the tab mounted on the flap.

The tab also was of two-piece construction. When the two parts of the tab were joined together with splice plates, it served as the AR = 2 tab; the inboard, two-hinge portion being used for the AR = 1 tab. In the AR = 2 configuration, it was possible to lock the outboard section of the tab to the flap, and still leave the inboard half of the tab free to be deflected. This was accomplished by bolting the middle tab bearing block to the inboard rib of the outboard tab panel. In Fig. 26b bolt A is shown in the locked condition. In the actual tests, two bolts were used.

Unlike the wing and flap construction, the tab spars were discontinuous and the ribs uninterrupted. The spar consisted of short segments of bent-up .040 in. 24ST sheet between each rib. The ribs were machined out of solid magnesium bar. Located between the tab hinges were two pairs of ribs of 3/8 in. stock separated by a 3/4 in. magnesium spacer. A fork-shaped rib was used at each hinge, the tines of the fork supporting the bearing shaft. A solid magnesium trailing edge piece was continuous along the span except for the break between the two portions of the tab. An .064 in. dural skin was riveted to the frame described above. Steel ballast weights were supported by the overhanging ribs to mass balance the tab as required.

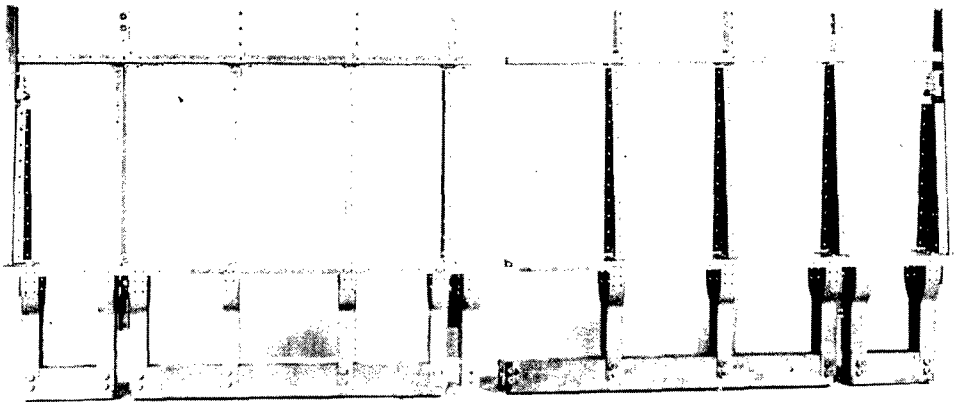

FIG. 23a FLAP UNCOVERED - SPLIT

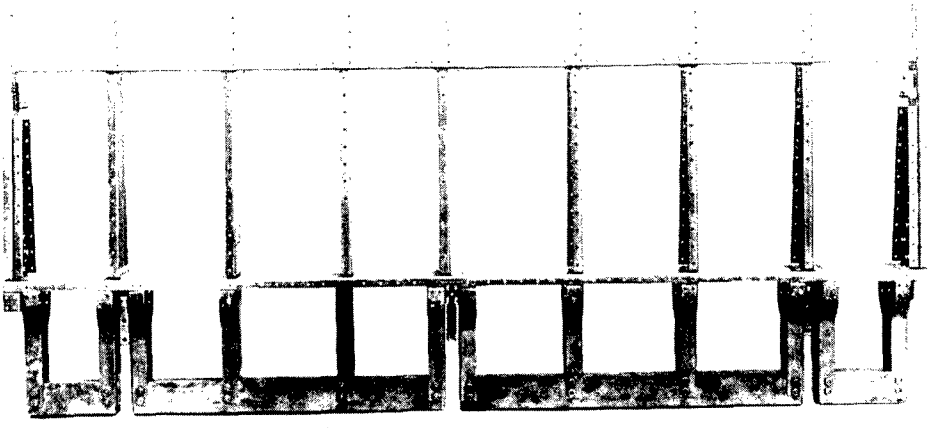

FIG. 23b FLAP UNCOVERED-JOINED

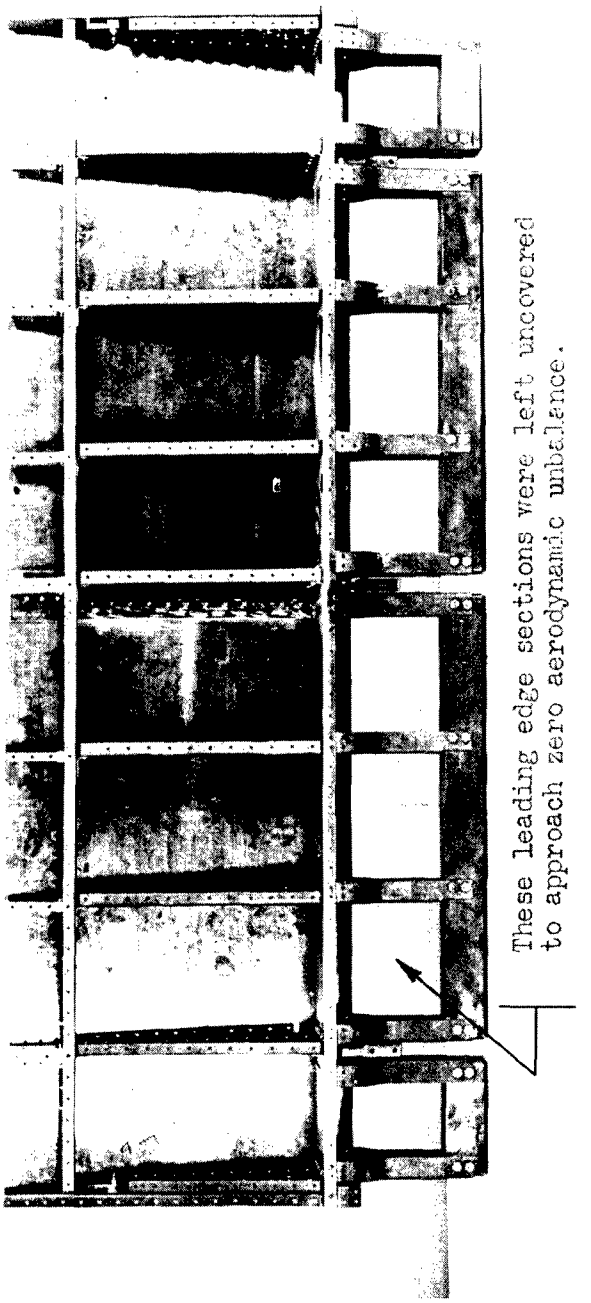

FIG. 24 FLAP PARTIALLY COVERED - JOINED

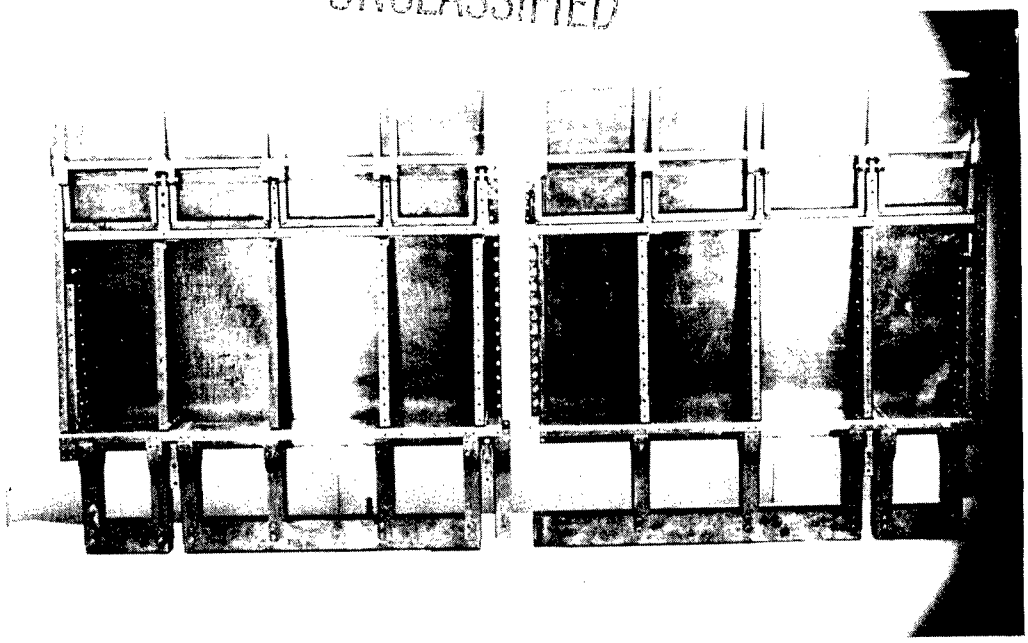

FIG. 25a FLAP & TAB - PARTIALLY COVERED - SPLIT

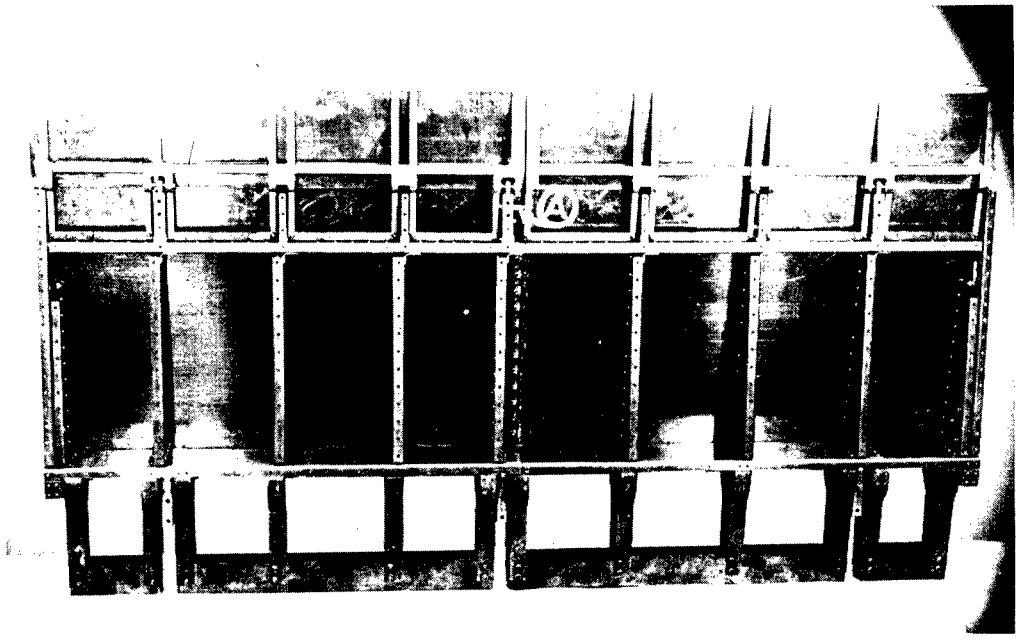

FIG. 25b FLAP & TAB - PARTIALLY COVERED - JOINED

Fig. 26 shows the tab in both its split and joined configuration. Fig. 25 illustrates how the tab was installed in the flap.

The end fitting (Fig. 27) transferred the model loads from the wing to the wing suspension system. A 1/4 in. steel plate attached to the end rib of the wing by twenty-two 1/4 in. machine screws served to transmit pitching moments from the model to the suspension system. To remove bending loads, two 3/4 in. steel legs were provided that attached to both skins with a pattern of twelve 5/16 in. machine screws. The torsion transmitting plate and bending transmitting legs described above attached to a spindle that fitted into the wing suspension system. The spindle slipped through head C, Figs. 28 and 29 into the two bearings retained therein.

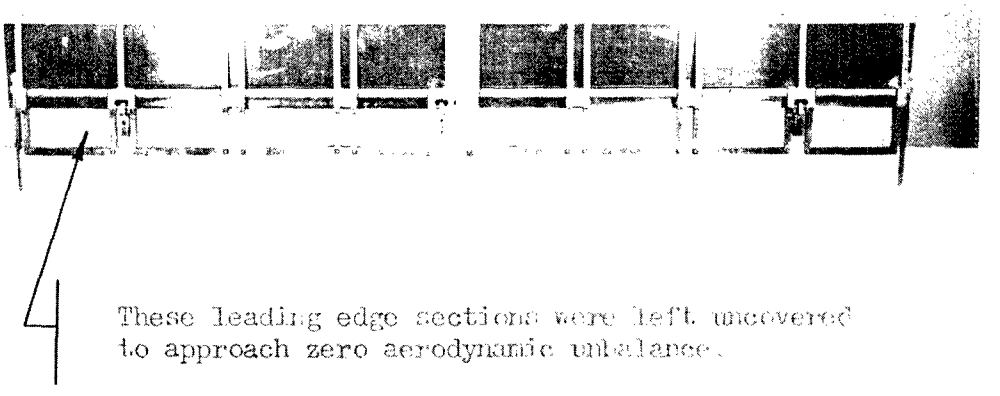

FIG. 26a TAB PARTIALLY COVERED-SPLIT

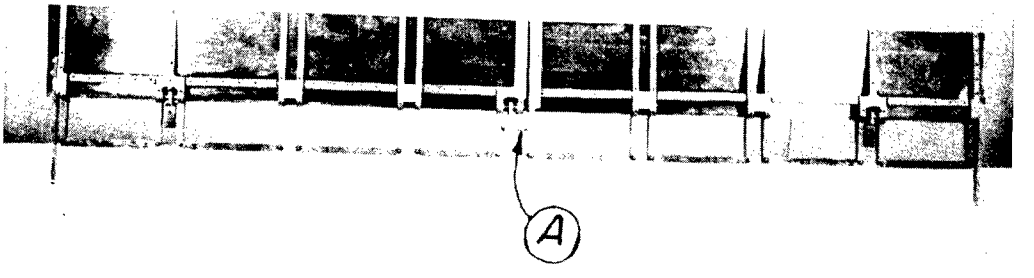

FIG. 26b TAB PARTIALLY COVERED-JOINED

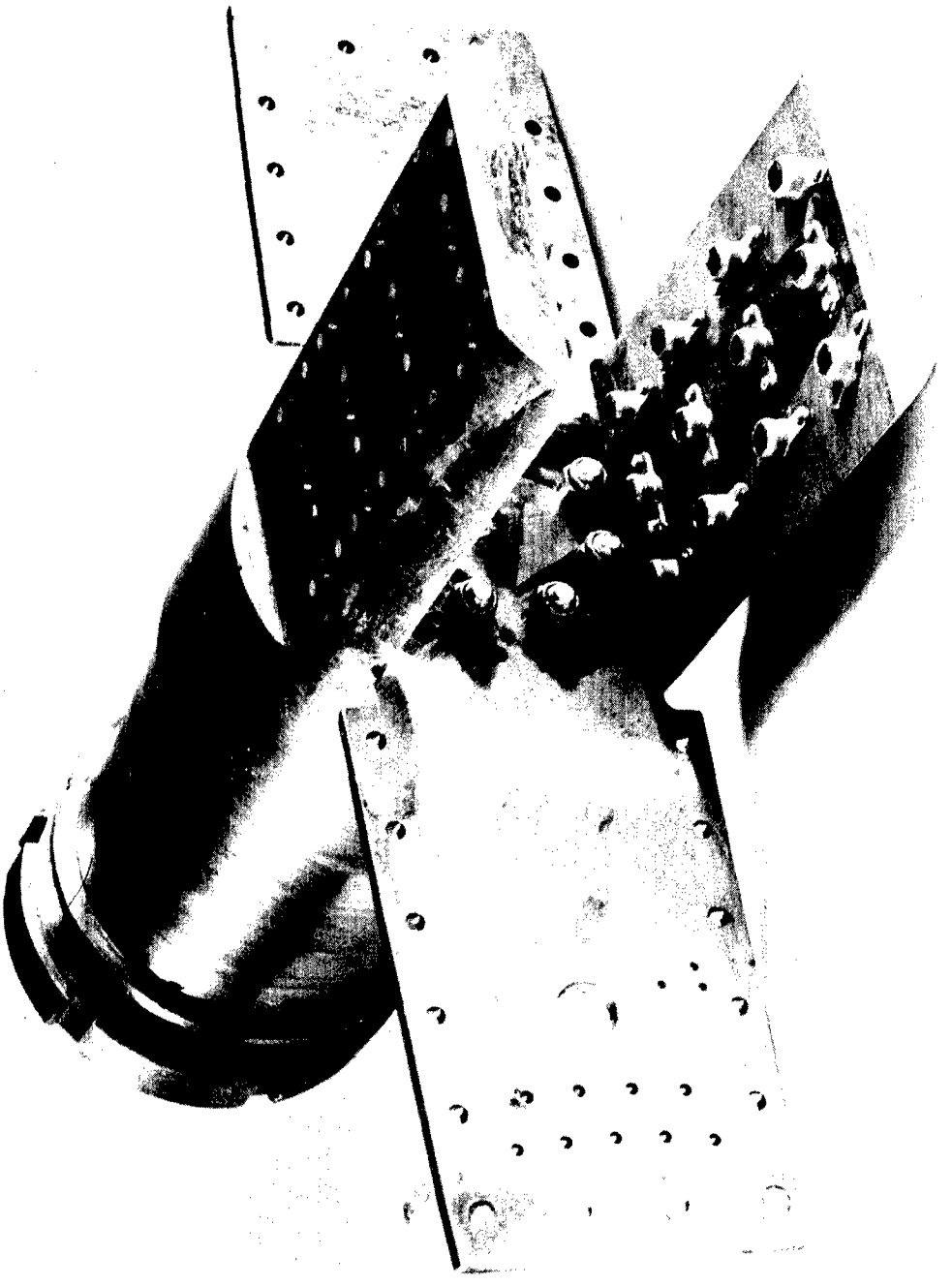

FIG. 27 WING END FITTING

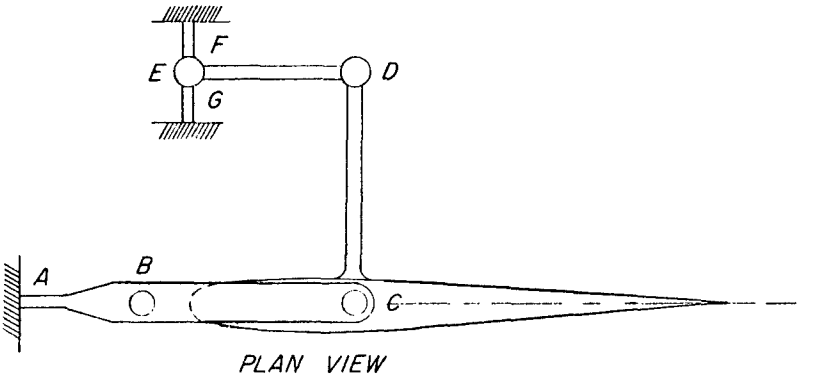

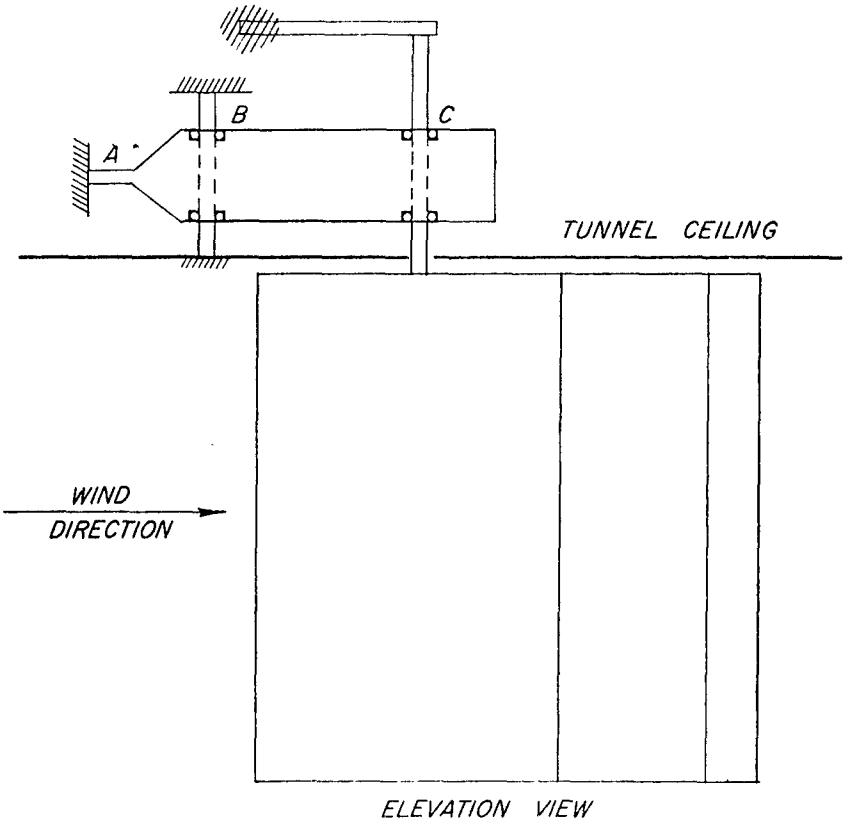

WING BALANCE SYSTEM

FIG. 28

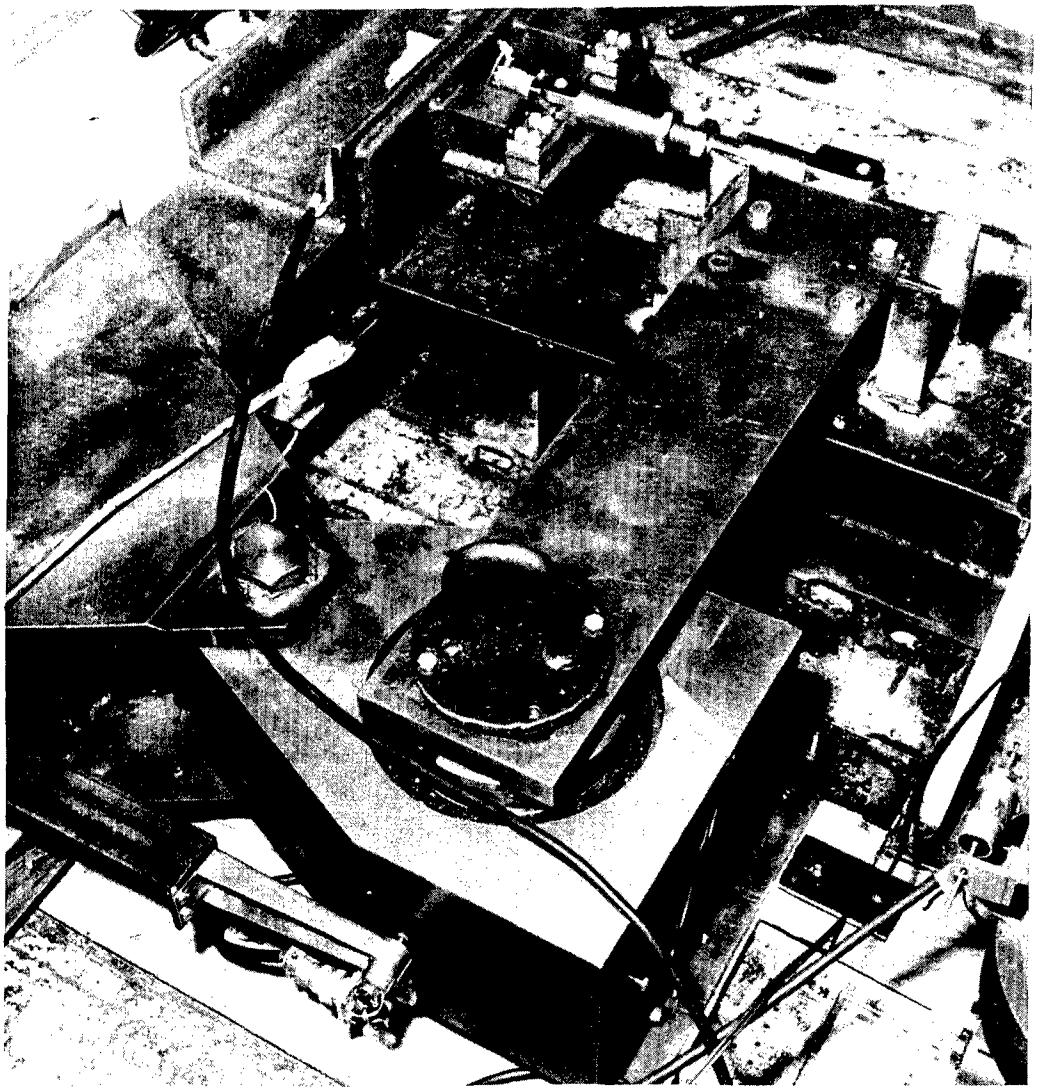

FIG. 29 WING SUSPENSION SYSTEM
TOP VIEW

APPENDIX II

INERTIA MOMENT BALANCING

A. Driven Surface

In every case the driven surface was statically mass balanced about its hinge line. This insured that there was zero shear force reacted by the hinge bearings at zero air speed. The balance was adjusted until no loads were indicated on the hinge carrying member (the wing when the flap was driven; the flap when the tab was driven), with the measuring equipment operating at full gain, while the driven surface was oscillated at various frequencies in the range of interest. Thus, with air on, the only loads carried across the hinge were of aerodynamic origin. As a double universal joint, incapable of transmitting shear, was provided in the input drive system all the aerodynamic shear was reacted by the hinges.

While the mass balancing of the driven surface reduced the total mechanical shear on the surface to zero, it did not, of course, assist in separating the mechanical hinge moment from the aerodynamic. The total hinge moment of the driven surface was reacted by the input drive system through the oscillator, a sensitive quill rod, and the universal joint. A Schaevitz pickup was used to measure the torsional deflection across the sensitive section and thus the total hinge moment. An accelerometer was mounted inside the driven surface at a distance from the hinge line so that its output was proportional to the angular acceleration of the surface. Obviously it was then also proportional to the mechanical (inertial) hinge moment. By suitable electrical mixing of the outputs of the Schaevitz and the accelerometer, a signal was obtained which was proportional only to the aerodynamic hinge moment, regardless of the amplitude and frequency of the driven surface's oscillation. The attenuators in the mixing circuit were adjusted so that at full gain of the measuring equipment the galvanometer that read hinge moment indicated no load with the driven surface oscillating in still air.

B. Locked Surface

When the flap was the driven surface, the tab was dynamically mass balanced with respect to its own and the flap's hinge lines. That is, sufficient mass was attached to the tab forward of its hinge line so that the product of inertia with respect to the two axes was zero. This insured that when the flap oscillated, there was zero mechanical tab hinge moment. Again the balance was adjusted so that no tab hinge

signal was obtained at full gain of the measuring equipment, with the flap oscillating.

With the tab the driven surface, there was no requirement on flap balance. Actually the flap was always left in its balance condition as required when it was the driven surface.

All balancing was done under ambient pressure conditions at zero air speed and therefore the oscillatory coefficients, as measured at speed, do not include the apparent mass terms; that is, the air loads induced on the model due to oscillations at zero air speed. Therefore, a small theoretical correction was applied to the measured loads to adjust for this lack. This correction was based on the results of Munk, Ref. 20, for elliptic wings. Munk tabulated factors that could be applied to the two-dimensional apparent mass to correct for finite aspect ratio. It was assumed herein that the same correction factor as developed for the elliptic wing could be applied to the rectangular wing. The correction factors used were 0.8 for AR = 2 and 0.6 for the AR = 1 wing. In all cases, however, the apparent mass contribution is only a very small part of the total oscillatory aerodynamic load.

APPENDIX III

SUSPENSION SYSTEM, LOCKING BARS, AND OSCILLATOR

A. Suspension System

Fig. 28 is a diagram of the wing suspension system which was to measure wing lift and pitching moments during part of the test program. The suspension separated the loads applied to the wing so that the bending moment in beam FG was proportional to the pitching moment and the bending moment in section AB of beam ABC was proportional to the wing lift. The suspension system was completely uncoupled. The wing pitching moment was obtained by measuring the deflection of beam FG at point E with a Schaevitz position indicator. The magnitude of the wing lift was obtained by measuring the bending moment in beam AB with a pair of resistance strain gages. The drag, rolling moment, and yawing moment on the model were reacted by balance beam ABC, carried by it to the bearings at B, and there transmitted to the fixed wind tunnel structure. Balance beam ABC was very stiff in the section B to C and these loads did not produce appreciable deflections. The method of reacting the pitching moment applied to the balance suspension system can be readily seen on Fig. 29. However, if the flap torque input system , Fig. 30, was in use while wing pitching moment was measured, an amount of torque equal to the hinge moment of the oscillating surface was transmitted through the input system and hence was not measured by the pitching moment beam. It was then necessary to add the flap hinge moment to the measured pitching moment to obtain the total pitching moment. Since the thirty per cent chord line was chosen as the elastic axis, it was also necessary to transfer the total moment obtained to the quarter chord line. No corrections of the lift measured by the balance were necessary as the attachments of the driving mechanism to the flap included a double universal joint through which there could be no transfer of shear loads. It was possible to lock out the wing suspension system to provide a rigidly mounted wing. A pattern of four 3/8 in. steel bolts tied beam CD to fixed structure to accomplish this.

B. Locking Bars

When one surface was being driven by the oscillator, the other was restrained from rotating by means of stiff locking bars, Fig. 6. Each locking bar was made of 1/4 in. steel plate. It was rigidly bolted to the surface being locked and attached to the locking surface by two taper pins. One taper pin was screwed to a fitting on the end

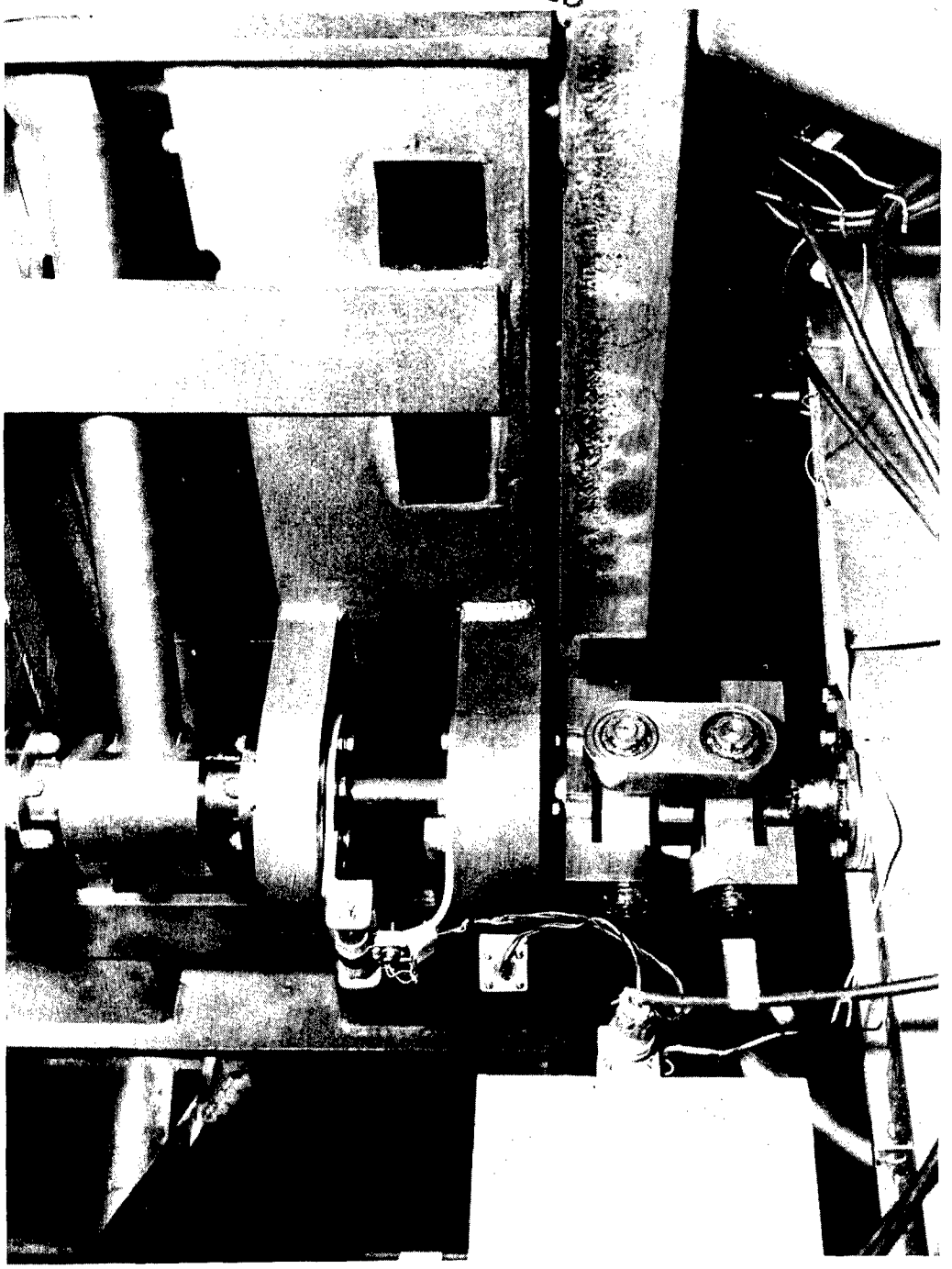

FIG. 30 TORQUE INPUT SYSTEM

rib of the locking surface; the other was driven through the locking bar and the end rib and held in place by friction. The locking bar was machined with a strain-sensitive section in the region of the hinge line on which the strain gages were mounted. The center line of the strain gages coincided with the hinge line of the locked surface as shown in Fig. 6.

For the AR = 2 model, two locking bars were used to restrain each full-span surface. One locking bar was located at the root; the other at the tip. In the case of AR = 1 model only one locking bar, located at the root, was used.

The flap and tab locking bars also provided a means of statically varying the angles of the respective control surfaces. The two taper pins, described above, were provided with a choice of mating holes from 0° to $\pm 8^{\circ}$ in 2° increments. Fig. 7 shows how the locking bars served to position the control surface.

As noted above when the flap was the driven surface, its hinge moment, as measured by the input system, had to be added to the wing moment as read by the wing suspension system, in order to get the total wing moment due to flap oscillation. Similarly when the tab was the driven surface, its hinge moment had to be added to the flap moment as read by the flap locking bars, in order to get the total flap hinge moment due to tab oscillation. (Wing moment data was not taken for the case of tab oscillating.)

C. Oscillator

The oscillator used in these tests is shown in the schematic diagram, Fig. 31. It was driven by a 2 hp induction motor through a Worthington variable speed drive unit, and a 9.75:1 fixed speed reducer, Fig. 32. A 114 lb-in^2 flywheel above the fixed reducer had an effective inertia of 10,800 lb-in^2 at the oscillator rpm. The output of the gear box was attached through a flexible coupling to the driver of the oscillator, member AB of Fig. 31. This had .15 in. eccentricity. A 22.375 in. connecting rod tied the follower to the driver, Fig. 30. The follower provided a choice of either 1.440 in. eccentricity or 2.200 in. eccentricity which gave 6° and 4° single amplitude oscillations respectively. The pins of the four-bar linkage were all provided with preloaded angular contact bearings.

The oscillator was so designed that the follower axis could be made coincident with either the flap or tab hinge lines so that it was possible to change the oscillator from driving the flap to driving the tab, or vice versa, very easily.

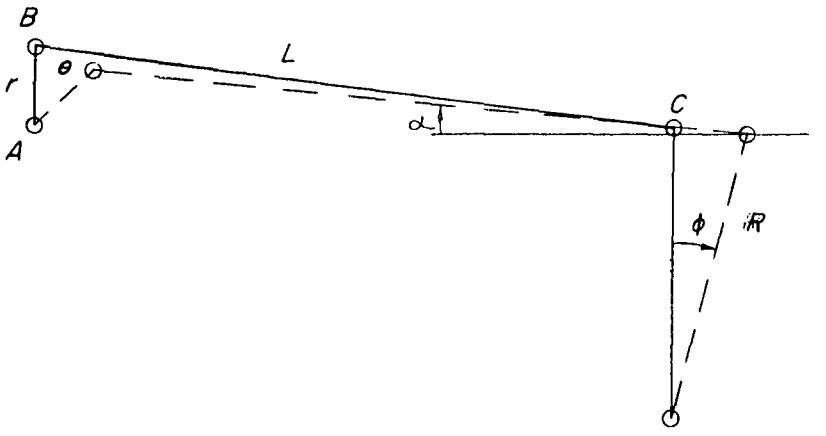

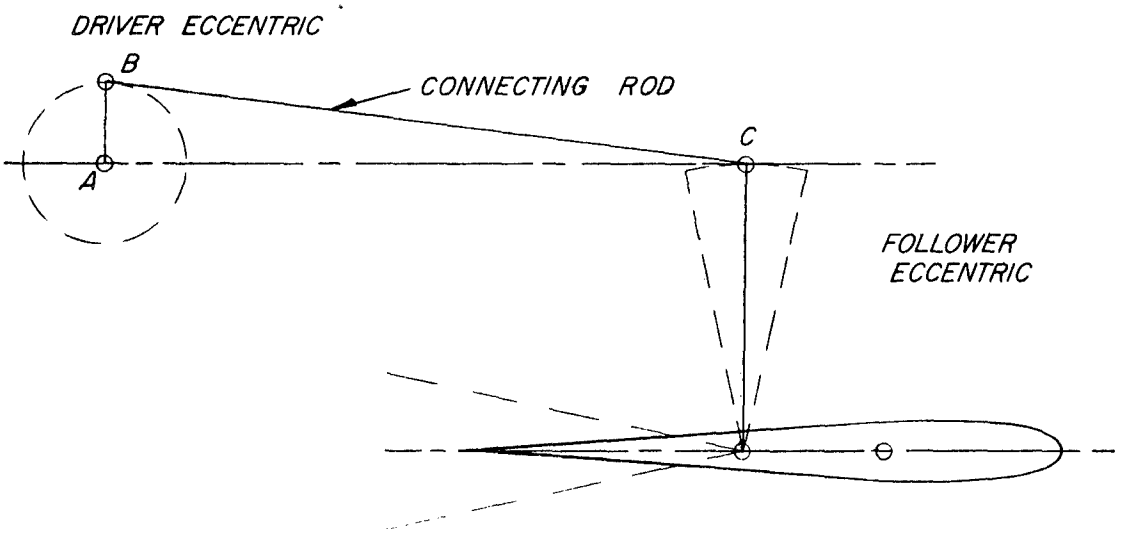

SCHEMATIC DIAGRAM OF OSCILLATOR
FIG. 31

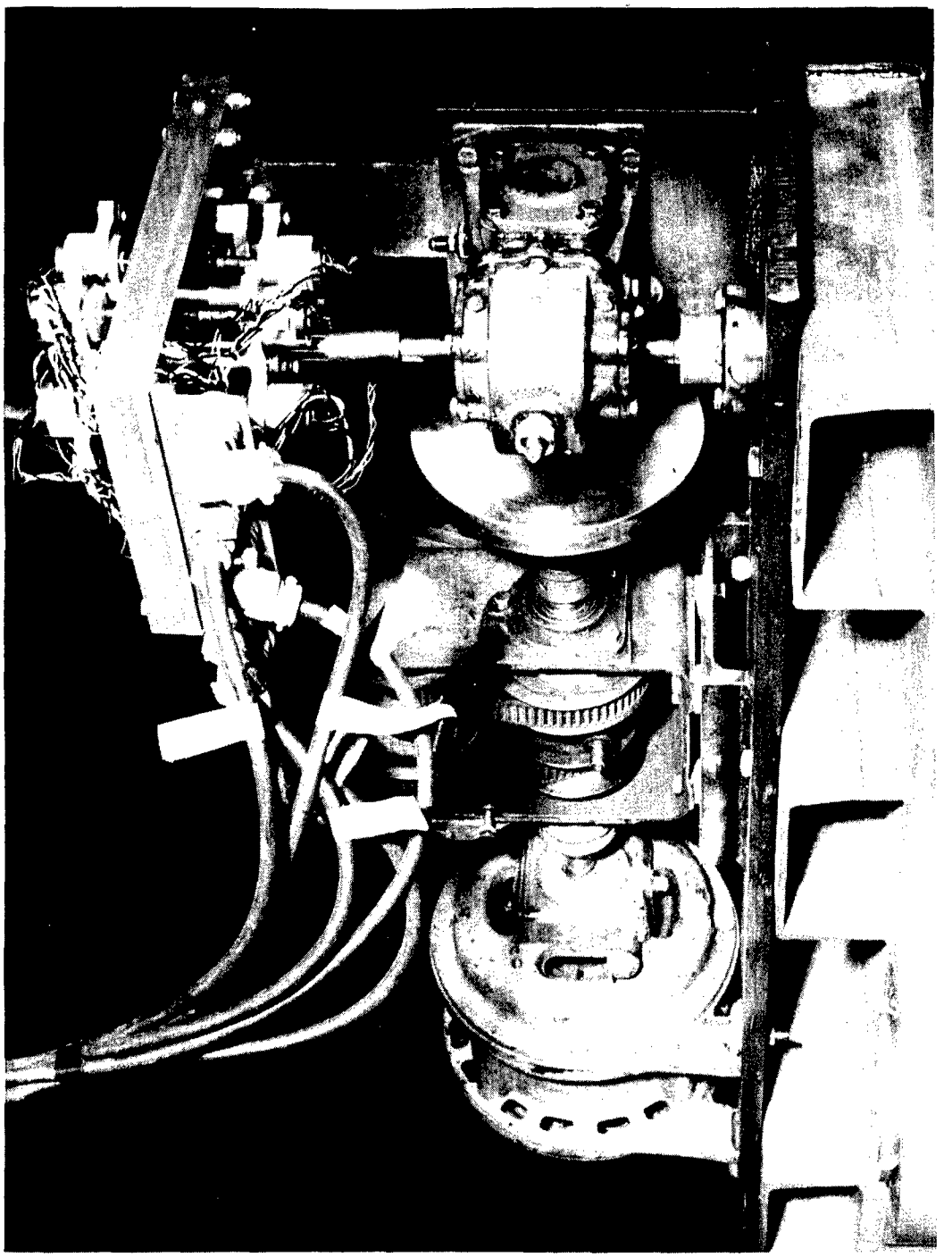

FIG. 32 OSCILLATOR DRIVE

The following is a kinematic analysis of the oscillator design. All the symbols used in the analysis are shown in Fig. 31.

The horizontal distances of the deflected linkage are summed and equated to the horizontal distance between the two pins, A and C.

$$r \sin\theta + L\cos\alpha - R\sin\phi = \sqrt{L^2 - r^2} \quad . \tag{1}$$

Similarly the vertical distances are summed

$$-r\cos\theta + L\sin\alpha + R\cos\phi = R \quad . \tag{2}$$

Solving (1) for $[L\cos\alpha]$ and (2) for $[L\sin\alpha]$, squaring both sides of the resulting equations and adding, we get:

$$\left[\sqrt{L^2 - r^2} + R\sin\phi - r\sin\theta\right]^2 + \left[r\cos\theta + R - R\cos\phi\right]^2 = L^2 \tag{3}$$

Expanding and simplifying equation (3)

$$R^2 + \sqrt{L^2 - r^2}\,(R\sin\phi) - R^2\cos\phi - \sqrt{L^2 - r^2}\,(r\sin\theta) + Rr\cos\theta - Rr\sin\phi\sin\theta - Rr\cos\phi\cos\theta = 0 \tag{4}$$

Making the small angle assumptions

$$\sin\phi = \phi$$

$$\cos\phi = 1.0$$

and solving for ϕ:

$$\phi = \frac{\sqrt{L^2 - r^2}\; r\sin\theta}{\sqrt{L^2 - r^2}\; R - Rr\sin\theta} \tag{5}$$

Dividing both numerator and denominator by $R\sqrt{L^2 - r^2}$

$$\phi = (r/R)\sin\theta \left[1 - \frac{r}{\sqrt{L^2 - r^2}}\sin\theta\right]^{-1}$$

This inverse term may be expanded as

$$\left[1 - x\right]^{-1} = \sum_{0}^{n} x^n$$

For the case of 6° single amplitude oscillations:

$r = .15$ in. $\quad L = 22.375$ in.
$R = 1.44$ in.

and

$$\phi = .104167 \sin\theta \left[1 + .006704 \sin\theta + .00004494 \sin^2\theta + \ldots\right]$$

or $$\phi = \left[.104167 \sin\theta + .000698 \sin^2\theta + .00000468 \sin^3\theta + \ldots\right].$$

Expressing $\sin^2\theta$ and $\sin^3\theta$ as a sum of linear higher harmonic terms:

$$\sin^2\theta = \tfrac{1}{2}(1 - \cos 2\theta)$$

$$\sin^3\theta = \tfrac{1}{4}(3\sin\theta - \sin 3\theta).$$

$$\phi = \Big\{\left[.104167 + .00000351 + \ldots\right]\sin\theta - \left[.00000117 + \ldots\right]\sin 3\theta + \left[.000349 + \ldots\right]\left[1 - \cos 2\theta\right] + \ldots \Big\}.$$

It is seen that the coefficient for each of the harmonics in the above series is itself expressed by an infinite series. However, the series for the coefficients converges very rapidly and can be approximated by the first few terms giving:

$$\phi = .000349 + .104518 \sin\theta - .000349 \cos 2\theta - .00000117 \sin 3\theta.$$

This series can be represented symbolically as

$$\phi = b_0 + a_1 \sin\theta + \sum_{k=2}^{\infty} a_k \sin(2k-1)\theta + \sum_{k=1}^{\infty} b_k \cos 2k\theta$$

and the harmonic distortion, D, can be computed by the following expression:

$$D = \sqrt{\frac{\int_0^{2\pi} (\phi - a_1 \sin\theta)^2 \, d\theta}{\int_0^{2\pi} a_1^2 \sin^2\theta \, d\theta}} = \frac{\sqrt{\sum_{k=2}^{\infty} (a_k)^2 + \sum_{k=1}^{\infty} (b_k)^2}}{a_1}$$

The constant term b_0 is ignored in computing the distortion since it merely introduces a small shift in the zero position. Substituting numerical values in the expression for the distortion:

$$D = \frac{\sqrt{(.000349)^2 + (.00000117)^2 + \ldots}}{.104518}$$

$$D = .00334$$

or $$D = .334\%$$

This is the inherent distortion of the oscillator mechanism. It is seen then that for practical purposes this distortion was effectively negligible.

APPENDIX IV

INSTRUMENTATION

The equipment used for this project was a Consolidated Engineering Corp., 1000 cycle carrier, system A, Fig. 33.

Eight channels of information were recorded as a function of time:

(1) Wing lift - Resistance strain gage
(2) Wing lift - Schaevitz type 18-L
(3) Wing pitching moment - Schaevitz type 18-L
(4) Flap torque input - Schaevitz type 14-L
(5) Tab torque input - Schaevitz type 14-L
(6) Flap locking moment - Resistance strain gage
(7) Tab locking moment - Resistance strain gage
(8) Position of oscillating surface - Accelerometer

A marker pulse was recorded to indicate when the model passed through neutral. Occasionally a 60 cycle trace was recorded to check the oscillograph timing oscillator. It was found that the timing lines represented .01075 seconds instead of the nominal .01 seconds.

The Schaevitz units were used as variable reluctance type pickups.

In the measurement of the torque input, it was necessary to subtract the inertia torque. The output of a Consolidated Engineering Corp. type 4-104 accelerometer mounted in the oscillating surface was mixed with the Schaevitz signal. This mixing was accomplished between the bridge and the amplifier. The outputs of the bridges were fed into the primaries of two similar transformers, the secondaries of which were connected in series and fed to an amplifier. The level of the output from the Schaevitz bridge was adjusted by means of a potentiometer until a minimum signal was observed in the oscillograph for a no-load condition (oscillations in still air).

The position of the oscillating surface was measured by an accelerometer mounted in the surface. The locking bars were instrumented with resistance strain gages. In the case of the AR = 2 model the top and bottom bars were connected in series.

As the fundamental frequency was of primary concern, it was desirable to suppress all higher harmonics and aerodynamic hash. This was accomplished by electrical filtering. The presence of the filters attenuated the signal considerably but was compensated for by using Consolidated Engineering type 7-115 (Flat $\pm 5\%$ 0-60 cps) galvanometers having a sensitivity of 13 micro-amperes per inch. Fig. 34 shows a typical oscillograph record.

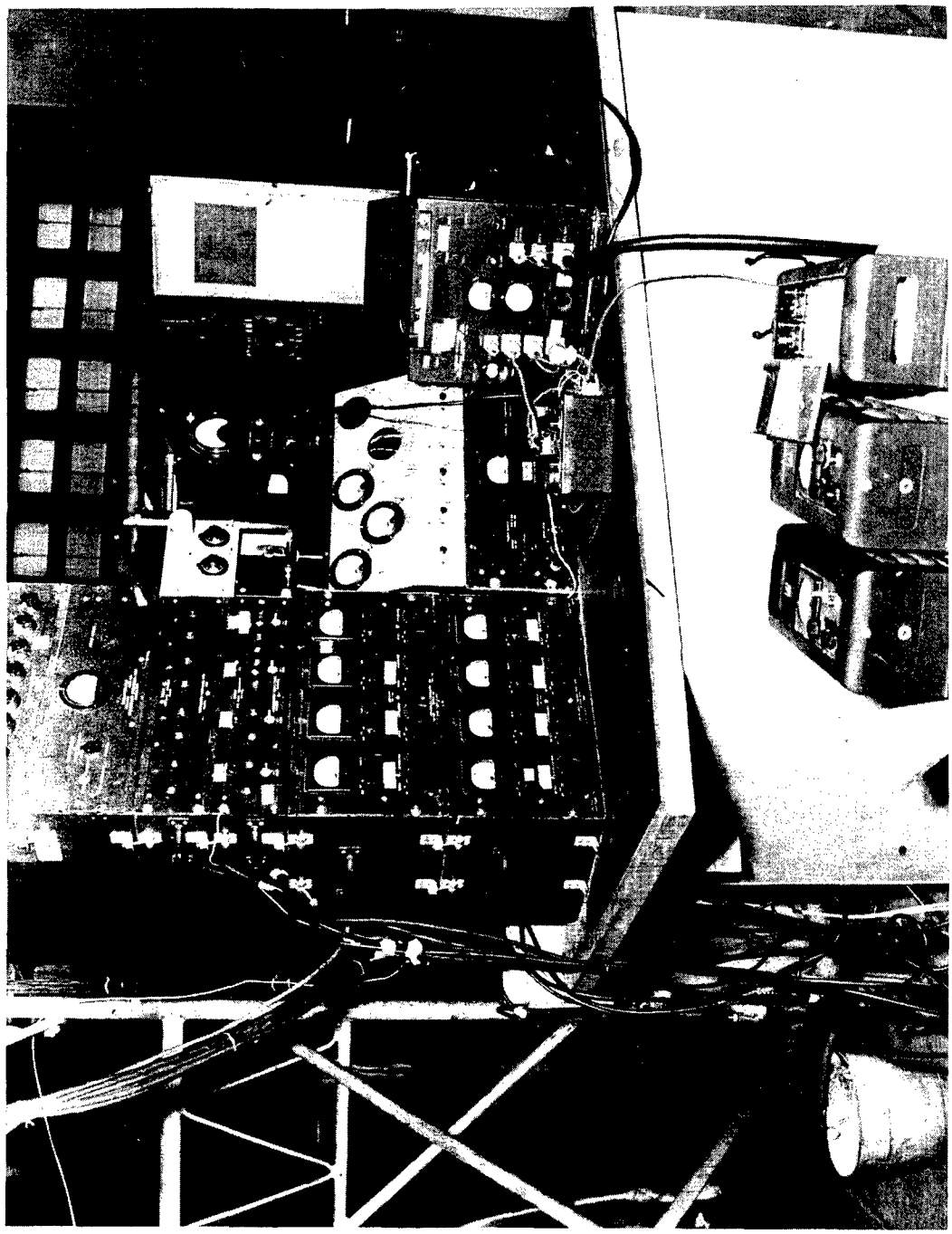

FIG. 33 INSTRUMENTATION

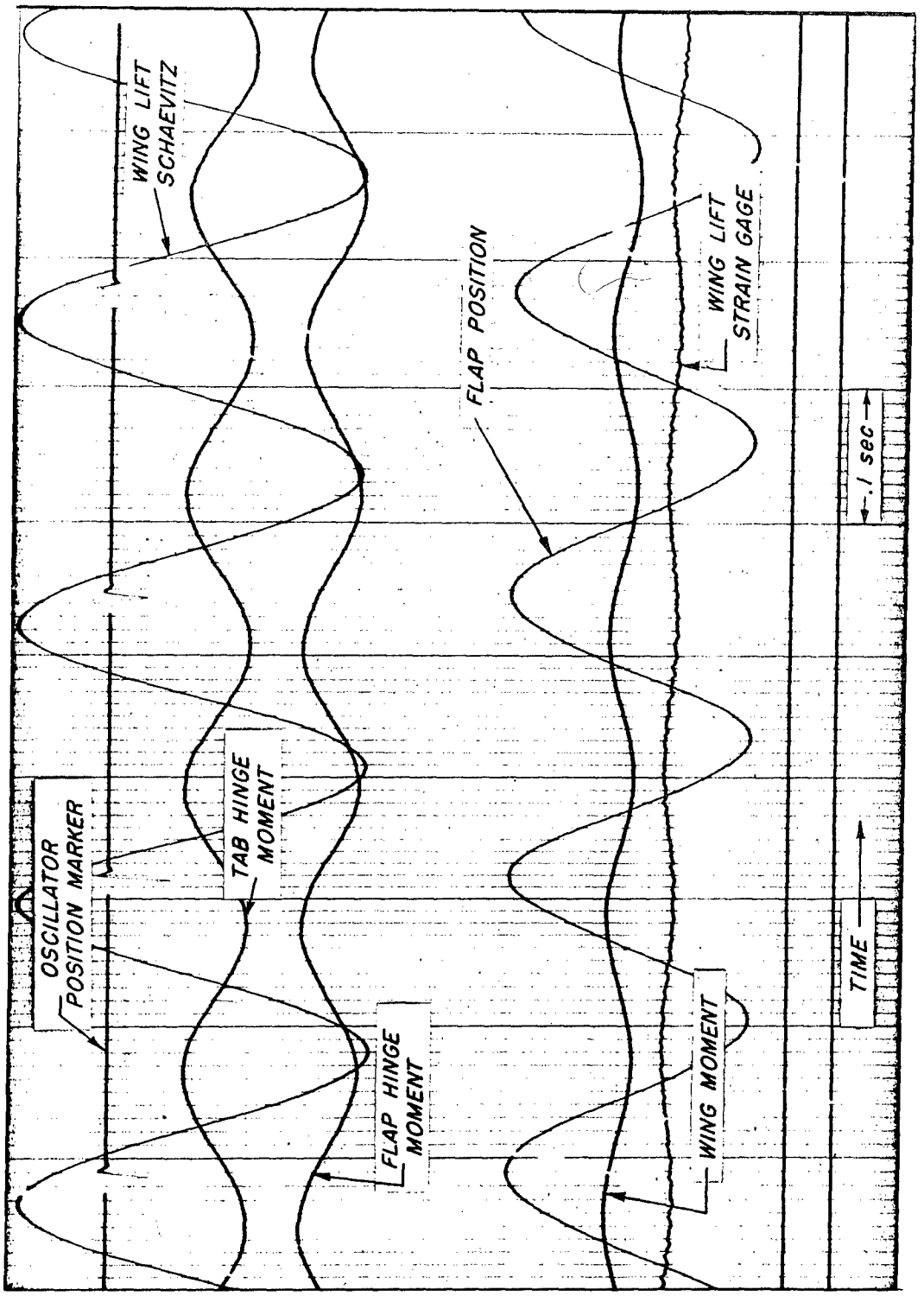

FIG. 34 TYPICAL OSCILLOGRAPH RECORD AR=1 WING UNLOCKED